The Astrophysical Journal, 569:720–741, 2002 April 20

OBSERVATIONAL MASS-TO-LIGHT RATIO OF GALAXY SYSTEMS FROM POOR GROUPS TO RICH CLUSTERS

Marisa Girardi, Patrizia Manzato, and Marino Mezzetti
Dipartimento di Astronomia, Università degli Studi di Trieste, Via Tiepolo 11, I-34131 Trieste, Italy;
girardi@ts.astro.it, manzato@ts.astro.it, mezzetti@ts.astro.it

Giuliano Giuricin[1]
Dipartimento di Astronomia, Università degli Studi di Trieste

and

Füsun Limboz
Istanbul University, Science Faculty, Astronomy and Space Science Department, 34452 Beyazit, Istanbul, Turkey
Received 2001 September 28; accepted 2001 December 27

ABSTRACT

We study the mass-to-light ratio of galaxy systems from poor groups to rich clusters and present for the first time a large database for useful comparisons with theoretical predictions. We extend a previous work, where B_j band luminosities and optical virial masses were analyzed for a sample of 89 clusters. Here we also consider a sample of 52 more clusters, 36 poor clusters, seven rich groups, and two catalogs, of ~500 groups each, recently identified in the Nearby Optical Galaxy sample by using two different algorithms. We obtain the blue luminosity and virial mass for all systems considered. We devote a large effort to establishing the homogeneity of the resulting values, as well as to considering comparable physical regions, i.e., those included within the virial radius. By analyzing a fiducial, combined sample of 294 systems we find that the mass increases faster than the luminosity: the linear fit gives $M \propto L_B^{1.34\pm0.03}$, with a tendency for a steeper increase in the low-mass range. In agreement with the previous work, our present results are superior owing to the much higher statistical significance and the wider dynamical range covered ($\sim 10^{12}$–10^{15} $M_\odot$). We present a comparison between our results and the theoretical predictions on the relation between M/L_B and halo mass, obtained by combining cosmological numerical simulations and semianalytic modeling of galaxy formation.

Subject headings: cosmology: observations — galaxies: clusters: general — galaxies: fundamental parameters

On-line material: machine-readable tables

1. INTRODUCTION

Since the work by Zwicky (1933), it is well known that the luminous matter associated with galaxies in clusters provides only a small part of the total cluster mass. The relative contribution of the dark matter component is usually specified in terms of the mass-to-light ratio, M/L, the total amount of mass relative to the total light within a given scale.

Pioneering analyses showed that M/L increases from the bright luminous parts of galaxies to cluster scales (Blumenthal et al. 1984). Indeed, models of biased galaxy formation, where galaxies formed only in the highest peaks in the initial fluctuation spectrum, naturally predict an increase of M/L with system mass (e.g., Bardeen et al. 1986; Davis et al. 1985). Several mechanisms whereby the efficiency of galaxy formation is biased toward very high density peaks are possible (e.g., Rees 1985). However, only recently has the combination of cosmological N-body simulations and semianalytic modeling of galaxy formation allowed realistic predictions about the M/L of galaxy systems (Kauffmann et al. 1999; Bahcall et al. 2000; Benson et al. 2000; Somerville et al. 2001). Although differing in details, it has been generally found that M/L increases with mass halo from very poor to rich systems, possibly with a flattening on large scales.

As for the observational point of view, the estimate of M/L in galaxy systems is not an easy task. Both mass and luminosity estimates are fraught with several uncertainties. The uncertainties in the luminosity determination are related to corrections for calibration of the photometry (when using inhomogeneous photometric data), background galaxy contamination, and the need to extrapolate the sum of measured luminosities of galaxy members to include faint galaxies and the outer parts of the systems, beyond the region studied (see, e.g., Oemler 1974).

Also the estimate of masses is not an easy task, in spite of the various methods that have been applied (e.g., Narayan & Bartelmann 1999; Schindler 1996; Mellier 1999; Biviano 2001). Masses of galaxy systems are inferred from either X-ray or optical data, under the general hypothesis of dynamical equilibrium. Estimates based on gravitational lensing do not require assumptions about the dynamical status of the system, but a good knowledge of the geometry of the potential well is necessary. Claims for a discrepancy (by a factor of 2–3) between cluster masses obtained with different methods cast doubts about the general reliability of mass estimates (e.g., Wu & Fang 1997). However, recent analyses have shown that, if we avoid cases of bimodal clusters, mass estimates concerning large cluster areas are in general agree-

[1] Deceased.

ment (Allen 1997; Girardi et al. 1998b, hereafter G98; Lewis et al. 1999).

Large collections of observational data concerning galaxies, groups, and clusters suggest that all systems have a constant ratio of $M/L_B \sim 200$–$300\ h\ M_\odot/L_\odot$ for scales larger than galaxies, so that the total mass of galaxy systems could be roughly accounted for by the total mass of their member galaxies, possibly plus the mass of the hot intracluster gas (Rubin 1993; Bahcall, Lubin, & Dorman 1995). Homogeneous samples, where both masses and luminosities are computed in a consistent way, would be more reliable. Unfortunately, the above observational difficulties prevented us from building a large M/L database spanning a wide dynamical range. Based on homogeneous optical data, the pioneering work by Dressler (1978) showed no evidence of correlation of M/L-values with richness for 12 clusters. More recently, David, Jones, & Forman (1995), who used homogeneous X-ray mass estimates and luminosities from different sources in the literature, showed that M/L_V of seven groups and clusters of galaxies are comparable. Also M/L_r-values for the sample of 15 clusters of the Canadian Network for Observational Cosmology (CNOC; Carlberg et al. 1996), where masses come from optical virial estimates, are consistent with an universal underlying value.

A slight increase of M/L with mass system was suggested by indirect analyses of the cluster fundamental plane, i.e., the study of the relations between cluster size, internal velocity dispersion, and luminosity (but see Fritsch & Buchert 1999). In fact, assuming the virialization state and internal structure of all clusters to be identical, one can derive the behavior of M/L. Working with a homogeneous photometric sample of 12 clusters, Schaeffer et al. (1993) found that $M/L_V \propto L_V^{0.3}$. Similarly, using homogeneous results for 29 clusters of the ESO Nearby Abell Cluster Survey (ENACS; Katgert et al. 1998), Adami et al. (1998a) showed that $M/L_{B_j} \propto \sigma_v$, where σ_v is the line-of-sight (LOS) velocity dispersion of member galaxies. This correlation was also directly verified by Adami et al. (1998b) in a following work by computing the projected virial masses.

Recently, Girardi et al. (2000, hereafter G00) faced the question from a direct point of view with a significant increment in the database statistics. They analyzed 89 clusters, all with homogeneous optical virial mass estimates by G98 and homogeneous luminosity estimates derived from the COSMOS catalog (Yentis et al. 1992). Moreover, the available data allowed the authors to compute mass and luminosity within the virial radius in order to analyze physically comparable regions in poor and rich clusters. Their main result is that the mass has a slight, but significant tendency to increase faster than the luminosity: $M \propto L_{B_j}^{1.2-1.3}$. Owing to the large uncertainties generally involved, it is really not surprising that such a slight effect could not be detected by previous analyses based on small statistics and/or a small dynamical range and/or inhomogeneous samples.

Recent support for G00 results came from a study of $\sim$ 200 galaxy groups, identified within the field galaxy redshift survey CNOC2 by Carlberg et al. (2001a), showing evidence that M/L increases with increasing σ_v. Moreover, M/L of CNOC2 groups proves to be smaller than that of CNOC clusters (Hoekstra, Yee, & Gladders 2001a). However, the question is still open. For example, Hradecky et al. (2000), who computed homogeneous X-ray mass and optical luminosity for eight galaxy systems, claimed that M/L_V is roughly independent of system mass.

New insights on the behavior of M/L for galaxy systems of different mass would be particularly useful in view of the theoretical predictions recently coming from cosmological N-body simulations combined with semianalytic modeling of galaxy formation. To draw more definitive conclusions about this topic, we extend the work of G00 by increasing the statistics of the database and doubling the dynamical range, from $\sim 5 \times 10^{13}$–$10^{15}\ h^{-1}\ M_\odot$ to $\sim 10^{12}$–$10^{15}\ h^{-1}\ M_\odot$. To this purpose, we consider both clusters analyzed by G98, the poor clusters by Ledlow et al. (1996, hereafter L96), the rich groups by Zabludoff & Mulchaey (1998a, hereafter ZM98), and the groups identified in the NOG sample (Nearby Optical Galaxy; Giuricin et al. 2000).

The paper is organized as follows. We describe the data samples in § 2. We compute the main observational quantities, i.e., virial masses and optical luminosities, for all galaxy systems in § 3. We devote § 4 to the analysis of the relation between mass and luminosity and to the mass-to-light ratio. We discuss our results in § 5, while in § 6 we give a brief summary of our main results and draw our conclusions.

Unless otherwise stated, we give errors at the 68% confidence level (hereafter c.l.).

A Hubble constant of 100 h km s^{-1} Mpc^{-1} is used throughout.

2. DATA SAMPLES

Table 1 briefly summarizes the samples of galaxy systems in this work. We list the sample name with the corresponding number of systems, N_S, and references for the catalog (cols. [1], [2], and [3], respectively); the subsample name with the corresponding number of systems, N_{SS} (cols. [4] and [5], respectively); the references for galaxy redshift and coordinates used for mass determination (col. [6]); the references

TABLE 1

SAMPLES OF GALAXY SYSTEMS

Name (1)	N_S (2)	Refs. (3)	Name$_{SS}$ (4)	N_{SS} (5)	Cord./z Refs.[a] (6)	Phot. Refs. (7)	Description (8)
CL	119	G98	C-CL	89	G98	COSMOS	Clusters (mainly ACO)
CL	119	G98	A-CL	52	G98	APS	Clusters (mainly ACO)
PS	43	L96, ZM98	C-PS	8	NED, ZM98	COSMOS	Poor clusters, rich groups
PS	43	L96,ZM98	A-PS	40	NED, ZM98	APS	Poor clusters, rich groups
HG	475	NOG			NOG	NOG	Loose groups
PG	513	NOG			NOG	NOG	Loose groups

[a] References for galaxy data are those which summarize information, e.g., the original redshift data for clusters come from ENACS and other literature: the reader can find them in G98.

for galaxy magnitudes used for luminosity determination (col. [7]); and a brief description of the sample (col. [8]). Detailed comments are given below.

2.1. *Cluster Sample* (*CL*)

The sample of nearby clusters ($z \leq 0.15$) of G98 is an extension of that of Fadda et al. (1996) and collects clusters having at least 30 galaxies with available redshifts in the field, in order to allow homogeneous and robust estimates of internal velocity dispersion and cluster mass. G00 have already analyzed a subsample of 89 clusters for which galaxy magnitudes are available in the COSMOS catalog (hereafter C-CL sample).

Here we select another 52 clusters (hereafter A-CL sample) for which galaxy magnitudes are available in the Revised APS catalog of POSSI (Pennington et al. 1993). In particular, we avoid the G98 clusters which show two peaks either in the velocity or in the projected galaxy distribution, as well as clusters with uncertain dynamics (cf. § 2 of G98). From the G98 analysis we take for each cluster: the LOS velocity dispersion σ_v, the cluster center, the virial radius $R_{\rm vir}$ (there called virialization radius), and the (corrected) virial mass M computed within $R_{\rm vir}$.

Among A-CLs, 22 systems are in common with C-CLs and will be used to homogenize the photometric data.

2.2. *Sample of Poor Systems* (*PS*)

The 71 poor galaxy clusters of L96 are a statistically complete sample derived from the catalog of 732 nearby poor clusters of White et al. (1999). The clusters of the original sample were optically selected by covering the entire sky north of -3° declination and are identified as concentrations of three or more galaxies with photographic magnitudes brighter than 15.7 (from the Zwicky et al. 1961–1968 catalog), possessing a galaxy surface overdensity of 21.5. The subsample of L96 is limited to the Galactic latitude range $|b| \geq 30^\circ$ and to the most dense and rich groups, i.e., with 46.4 surface-density enhancement and with at least four Zwicky galaxies. L96 collected new redshifts and computed velocity dispersions for several of these poor clusters.

The sample of ZM98 consists of 12 nearby optically selected groups from the literature (NED, NASA/IPAC Extragalactic Database) for which there are existing, sometimes serendipitous, pointed PSPC observations of the fields in which the groups lie. As pointed out by the authors, this group sample is not representative of published group catalogs but is weighted toward X-ray groups. By using multifiber spectroscopy, ZM98 extend greatly the number of galaxies with available redshift and present a sample of 1002 galaxy velocities.

Avoiding poor systems with $z \lesssim 0.01$, more strongly affected by peculiar motions, and those which do not survive our procedure of member selection (cf. § 3.1), we consider 36 poor clusters and seven rich groups for a total sample of 43 poor systems (hereafter PSs) having available magnitudes in COSMOS and/or APS (C-PS and A-PS samples, respectively). In particular, five poor systems have available magnitudes in both photometric catalogs.

From ZM98 we take for each rich group: the group center, and galaxy positions and redshifts, to apply our procedure of member selection (cf. § 3.1). From L96 we take the mean velocity and the center for each poor cluster: we use these data to collect galaxy positions and redshifts within $1.5\,h^{-1}$ Mpc from the cluster center by using NED, and then apply our procedure of member selection.

2.3. *NOG Group Samples* (*HG and PG*)

We use the groups identified by Giuricin et al. (2000) in the NOG sample. This is a complete, distance limited ($cz < 6000$ km s^{-1}) and magnitude limited ($B \leq 14$) sample of $\sim$7000 optical galaxies, which covers about 2/3 of the sky ($|b| > 20^\circ$), and appears to be quasi-complete in redshift (97%). The authors identified the groups by means of both the hierarchical and the percolation "friend-of-friend" methods: their final catalogs contain 475 and 513 groups, respectively (hereafter HG and PG).

From Giuricin et al. (2000) we take the data available for each group's galaxy positions, redshifts, and corrected total blue magnitudes.

3. MASS AND LUMINOSITY ESTIMATES

With the exception of the masses of CLs and luminosities of C-CLs, all other mass and luminosity estimates are obtained in this study. In order to extend the work by G00 throughout this section, a great effort is devoted to computing masses and luminosities in a consistent way so as to obtain a large homogeneous sample of M/L estimates.

In particular, G00 used mass and luminosity computed within the virial radius $R_{\rm vir}$, which defines, as usual in the context of cold dark matter (CDM) cosmologies, the region where the matter overdensity is $\sim$180 for a $\Omega_m = 1$ cosmology, or $\sim$350 for a $\Omega_m = 0.3$ and $\Omega_\Lambda = 0.7$ cosmology (which hereafter we use as our reference model in this study). In this region one can assume a status of dynamical equilibrium and therefore reasonably apply the virial theorem for the mass computation.

In our case, where we deal with systems spanning a large dynamical range, to consider comparable physical regions is particularly useful for mass and luminosity estimation. The great advantage lies both in considering a similar dynamical status (e.g., in the case of variations among galaxy systems, cf. Zabludoff & Mulchaey 1998b) and a comparable galaxy population (in connection with color gradients, e.g., Abraham et al. 1996). Therefore, we compute both mass and luminosity within $R_{\rm vir}$.

3.1. *Mass Determination*

For poor systems, PCLs, we perform the same procedure already used by G98, in particular with those recipes for poor data samples already introduced by Girardi & Mezzetti (2001). Since the procedure was already amply described in these works (cf. also Fadda et al. 1996), here we only outline the main steps.

3.1.1. *Member Selection*

After having converted all galaxy velocities to galactocentric ones, we perform the selection of member galaxies. First, we apply the one-dimensional algorithm of the adaptive kernel technique by Pisani (1993, see also Appendix A of Girardi et al. 1996) to find the significant peaks in the velocity distribution. The main cluster body is generally identified as the highest significant peak. In some particular cases, where the sampling is particularly poor, we had to choose another peak in order to have a good coincidence (at least within 1000 km s^{-1}) with the mean system velocity sug-

gested by L96. All galaxies not belonging to the selected peak are rejected as non cluster members. Fadda et al. (1996) and G98 required that peaks must be significant at the 99% c.l., but in dealing with poor sampled systems we follow the suggestion by Girardi & Mezzetti (2001), considering peaks having smaller significance, less than 99% (but generally greater than 95%). We do not consider systems with multipeaked velocity distributions.

Afterward, we use the combination of position and velocity information to reveal the presence of surviving interlopers by applying the "shifting gapper" (Fadda et al. 1996). We reject galaxies that are too far away in velocity (by $\geq$1000 km s^{-1}) from the main body of galaxies at a given distance from the system center (within a shifting annulus of 0.4 h^{-1} Mpc or large enough to include 15 galaxies). As for very poor samples with less than 15 members, we reject galaxies that are too far away in velocity from the main body of galaxies of the whole system.

At this point we recompute the system center for rich groups of ZM98 (by using the two-dimensional adaptive kernel method; cf. Pisani 1996; Girardi et al. 1996), while for the poor clusters of L96 we retain the original centers, generally coming from a much larger number of galaxies.

3.1.2. *Galaxy Velocity Dispersion*

We estimate the "robust" LOS velocity dispersion, σ_v, by using the biweight and the gapper estimators when the galaxy number is larger or smaller than 15, respectively (cf. ROSTAT routines—see Beers, Flynn, & Gebhardt 1990), and applying the relativistic correction and the usual correction for velocity errors (Danese, De Zotti, & di Tullio 1980). For the poor clusters of L96, where redshifts are taken from NED, we assume a typical velocity error of 100 km s^{-1}.

Following Fadda et al. (1996, cf. also Girardi et al. 1996) we analyze the "integral" velocity dispersion profile (hereafter VDP), where the dispersion at a given (projected) radius is evaluated by using all the galaxies within that radius, i.e., $\sigma_v(<R)$. The VDPs make it possible for us to check the robustness of the σ_v estimate. In fact, the presence of velocity anisotropy in galaxy orbits can strongly influence the value of σ_v computed for the central cluster region but does not affect the value of the σ_v computed for the whole cluster (e.g., Merritt 1988). The VDPs of nearby clusters show strongly increasing or decreasing behaviors in the central cluster regions, but they are flattening out in the external regions, suggesting that in such regions they are no longer affected by velocity anisotropies. Thus, while the σ_v-values computed for the central cluster region could be a very poor estimate of the depth of cluster potential wells, one can reasonably adopt the σ_v-value computed by taking all the galaxies within the radius at which the VDP becomes roughly constant.

When the data are good enough, also poor systems show a (asymptotical) flatness in their VDPs (see Fig. 1). However, some cases show a sharp increase toward the very external regions, suggesting the presence of a neighboring system with a different mean velocity (cf., e.g., A3391 and A3395 in Girardi et al. 1996). Since the radius of our data samples is relatively large this situation is not unexpected. For these systems, we assume that the real system is enclosed within the radius where the VDP sharply increases when there are enough galaxies to detect a region of a flat profile (N79-298, N79-283, N67-336, N45-363) or, otherwise, within the first galaxy useful for computing σ_v (S49-142, N67-317).

G98 computed the virial radius from

$$R_{\rm vir} = [2 \times \sigma_v/(1000 \text{ km s}^{-1})]\ h^{-1} \text{ Mpc}\ , \qquad (1)$$

and we adopt the same definition. Indeed, this is only a first-order approximation, but Girardi et al. (1998a) made a recomputation for some choices of cosmological models: they found that, for our reference model ($\Omega_m = 0.3,\ \Omega_\Lambda = 0.7$), the difference is $\sim$10% for $R_{\rm vir}$ and $\sim$5% for the mass within $R_{\rm vir}$. Since we are interested in fixing a radius for dealing with consistent physical regions in different systems, rather than with precise cosmological computations, this choice is well suited to our aims.

3.1.3. *Galaxy Spatial Distribution*

In order to estimate the virial mass, one must compute the radius appearing in the virial theorem (Limber & Mathews 1960), which is, indeed, larger than the harmonic radius by about a factor of 2. In particular, since we want to compute the mass within $R_{\rm vir}$, only the N galaxies within $R_{\rm vir}$ are considered. Here we use the luminosity-unweighted, projected version of this radius, $R_{\rm PV}$ (cf. Giuricin, Mardirossian, & Mezzetti 1982; please note that G98 referred to $R_{\rm PV}$ as "virial radius"):

$$R_{\rm PV} = N(N-1)/(\Sigma_{i>j} R_{ij}^{-1})\ , \qquad (2)$$

where R_{ij} are the projected mutual galaxy distances.

Unfortunately, for several poor systems the number of galaxies within $R_{\rm vir}$ is very small ($N \leq 6$) or the sampled region is smaller than $R_{\rm vir}$ (26 systems). In these cases the estimate of $R_{\rm PV}$ can be recovered in an alternative way from the knowledge of the galaxy surface density profile $\Sigma(R)$: Girardi et al. (1995) presented this method for the King-like distribution $\Sigma(R) = \Sigma(0)/[1 + (R/R_c)^2]^\alpha$, where R_c is the core radius and α is the parameter which describes the galaxy distribution in external regions (cf. the β-profile used in X-ray surface brightness analyses).

The alternative procedure described by Girardi et al. (1995) allows one to compute $R_{\rm PV}$ at each radius and, in particular, we compute $R_{\rm PV}$ at $R_{\rm vir}$. Here we use the same parameters as the King-like distribution already used by G98: $\alpha = 0.7$ and $R_c/R_{\rm vir} = 0.05$. In fact, by using the 17 systems sampled with $N \leq 10$ galaxies within $R_{\rm vir}$ and the same maximum likelihood approach, we fit consistent values. We find: $\alpha = 0.64^{+0.07}_{-0.02}$ (median value and 90% errors), which corresponds to a galaxy volume-density of $\rho \propto r^{-2.4}$ for $R \gg R_C$; and $R_c/R_{\rm vir} = 0.03^{+0.03}_{-0.01}$.

3.1.4. *Virial Mass*

Assuming that clusters are spherical, nonrotating systems, and that the internal mass distribution follows galaxy distribution, cluster masses can be computed with the virial theorem (e.g., Limber & Mathews 1960; The & White 1986) as

$$M = M_V - C = \frac{3\pi}{2} \times \frac{\sigma_v^2 R_{\rm PV}}{G} - C\ , \qquad (3)$$

where the C correction takes into account that the system is not fully enclosed within the boundary radius, b, here $R_{\rm vir}$.

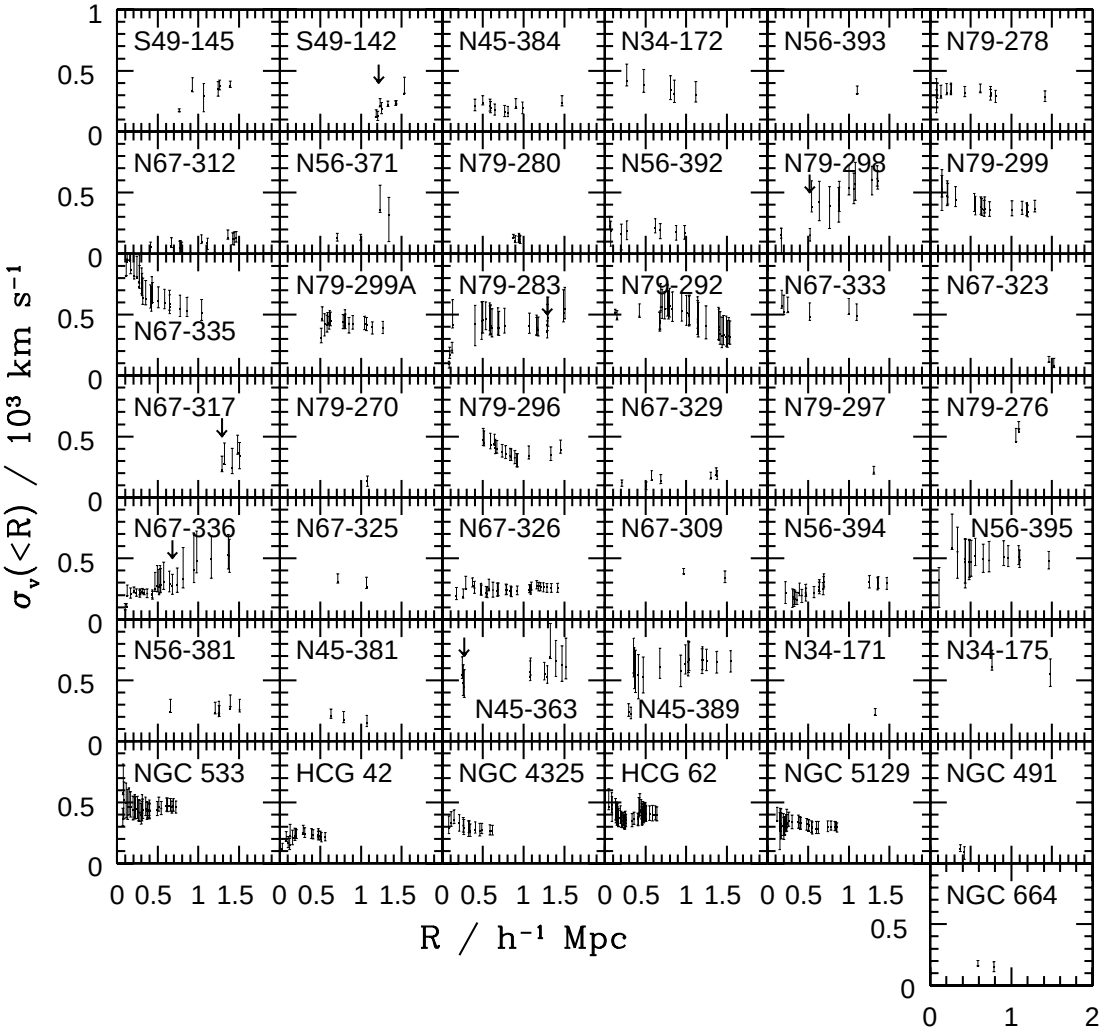

FIG. 1.—Integrated line-of-sight velocity dispersion profiles $\sigma_v(< R)$, where the dispersion at a given (projected) radius from the system center is estimated by considering all galaxies within that radius. The bootstrap error bands at the 68% c.l. are shown. The arrows indicate where six clusters are truncated according to the analysis of velocity dispersion profiles (see text).

The correction can be written as

$$C = M_V \times 4\pi b^3 \frac{\rho(b)}{\int_0^b 4\pi r^2 \rho\, dr} [\sigma_r(b)/\sigma(< b)]^2 \qquad (4)$$

and requires knowledge of the velocity anisotropy of galaxy orbits. In fact, $\sigma_r(b)$ is the radial component of the velocity dispersion $\sigma(b)$, while $\sigma(< b)$ refers to the integrated velocity dispersion within b; here $b = R_{\rm vir}$.

In order to give the C-correction for each individual cluster, G98 used a profile indicator, I_p, which is the ratio between $\sigma_v(< 0.2 \times R_{\rm vir})$, the LOS velocity dispersion computed by considering the galaxies within the central cluster region of radius $R = 0.2 \times R_{\rm vir}$, and the global σ_v. According to the values of this parameter, they divided clusters into three classes: "A" clusters with a decreasing profile ($I_p > 1.16$), "C" clusters with an increasing profile ($I_p < 0.97$), and an intermediate class "B" of clusters with very flat profiles ($0.97 < I_p < 1.16$). Each of the three types of profiles can be explained by models with a different kind of velocity anisotropy: fully isotropical (B), with a radial component only in external regions (A), or with a circular component in central regions (C); cf. Figure 3 of G98 and relative comments.

In the same way, we can define six, four, and five systems belonging to class A, B, and C, respectively, and for each class we use the respective value $[\sigma_r(R_{\rm vir})/\sigma(< R_{\rm vir})]^2$ and typical galaxy distribution $\rho(r)$ to determine the C-corrections. For systems where we cannot define the type of profile we assume isotropical velocities, i.e., the type "B", already shown to be the most adequate for describing clusters and acceptable also for poor clusters (at the 39% χ^2 probability). Figure 2 compares the observational velocity dispersion profile $\sigma_v(R)$, as computed by combining together the galaxies of all 17 "well-sampled" systems, to the three models with different velocity anisotropy recovered by using the Jeans equation: both the model with isotropical velocity and that with circular velocity anisotropy are acceptable.

The median value of the correction of the sample is 20%, similar to that of G98, and also to that of CNOC clusters (Carlberg, Yee, & Ellingson 1997).

Table 2 lists the results of the dynamical analysis: the system name (col. [1]); N_f, the number of galaxies with measured redshift in each cluster field (col. [2]); N_m, the number

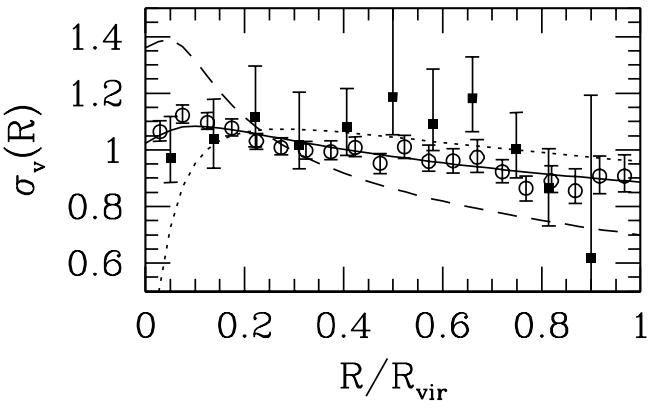

FIG. 2.—The (normalized) line-of-sight velocity dispersion, $\sigma_v(R)$, as a function of the (normalized) projected distance from the system center. The points represent data combined from all systems and binned in equispatial intervals. We give the robust estimates of velocity dispersion and the respective bootstrap errors. We give the results for poor systems (*filled circles*) and for nearby clusters taken from Girardi et al. (1998b, *open circles*). The solid, dotted, and dashed lines represent models with different kinds of velocity anisotropy: isotropic, circular in central regions, and radial in external regions, respectively (see text).

of member galaxies after checking with VDP (col. [3]) and used to compute V, the mean velocity (col. [4]), and σ_v, the global LOS velocity dispersion, with the respective bootstrap errors (col. [5]): only systems with $N_m \geq 5$ are retained in the sample; $R_{\rm vir}$, the virial radius which defines the region of dynamical equilibrium (col. [6]); N, the number of member galaxies within $R_{\rm vir}$ (col. [7]); $R_{\rm PV}$, the projected radius used in the virial theorem and here computed within $R_{\rm vir}$, with the respective jackknife error (a 25% error is assumed for radii computed from the alternative theoretical formula; cf. G98) (col. [8]); T, the type of velocity dispersion profile (col. [9]); M, the virial mass contained within $R_{\rm vir}$ after pressure surface term correction with the corresponding errors [col. (10)]. The percent errors on M are the same as for M_V, i.e., we take into account the errors on σ_v and $R_{\rm PV}$ and neglect the uncertainties on C-correction.

The median percent error on mass is ~40% but varies with the mass (see also Girardi et al. 1998a), ranging from ~30% for massive systems, $M > 5 \times 10^{14}\ M_\odot$, to ~75% for less massive systems, $M < 5 \times 10^{13}\ M_\odot$.

Finally, we note that four poor clusters here analyzed were already studied by G98: N34-172/MKW1, N67-312/MKW10, N67-335/MKW4, N67-336/MKW12. The two mass estimates, based on partially different data samples (G98 considered only homogeneous data from specific cluster studies), show fair agreement.

3.2. *Luminosity Determination*

3.2.1. *COSMOS and APS Catalogs*

Following G00, we derive from the COSMOS catalog the magnitudes for eight poor systems of the PS sample.

The COSMOS catalog is described by Yentis et al. (1992), and a part, the Edinburgh-Durham Southern Galaxy Catalog (EDSG) is well analyzed by Heydon-Dumbleton, Collins, & MacGillivray (1989). The EDSGC is nominally quasi-complete to $B_j = 20$. A more conservative limiting apparent magnitude was suggested by Valotto et al. (1997), who found that galaxy counts follow a uniform law for $B_j < 19.4$. Accordingly, and following G00, we decide to adopt a limiting magnitude of $B_j = 19.4$ for the COSMOS catalog. Within this limit, we adopt a completeness value of 91% for areas containing galaxy systems, suggested as being more appropriate for areas of high surface density (Katgert et al. 1998) and the nominal 95% completeness value for the rest of the catalog (Heydon-Dumbleton et al. 1989). These levels of incompleteness are assumed for all magnitudes down to $B_j = 19.4$, since Katgert et al. (1998) found that the magnitude distribution of missing galaxies is essentially the same as for sampled galaxies. Moreover, we note that, although COSMOS magnitudes are isophotal magnitudes, the threshold on average being only 8% above the sky (Heydon-Dumbleton, Collins, & MacGillivray 1988) the difference between COSMOS magnitudes and "total" magnitudes becomes significant only at the faint limit (well below our limiting magnitude; cf. Shanks, Stevenson, & Fong 1984).

For each system of C-PS we select galaxies with magnitudes $B_j < 19.4$ within circular regions with a radius equal to $R_{\rm vir}$ and a center as chosen in § 3.1.1.

Moreover, we take magnitudes for 52 CLs and 40 PSs from the fields which are currently on-line from the APS Revised Catalog of POSS I.

The APS Catalog is the result of scans of glass duplicates of the blue (O) and red (E) plates of the original Palomar Observatory Sky Survey (POSS I) for all 664 fields with $|b| > 20°$. The operation of the Automated Plate Scanner (APS) and the scanning procedures and parameters are described in detail in Pennington et al. (1993). Here we consider $B_{\rm APS}$ band-magnitude, corresponding to the (O) Sky Survey plates, which is an isophotal magnitude within the level of surface brightness of $\mu \sim 26.5$ mag per square arcsec. Comparisons with available photometry in de Vaucouleurs et al. (1991) and for fainter galaxies at the North Galactic Pole find that APS-derived integrated galaxy magnitudes show no systematic photometric errors and a typical rms scatter of 0.2 to 0.3 mag (Odewahn & Aldering 1995). Several checks suggest that the catalog is quasi-complete for $B_{\rm APS} < 19$–20 mag (Odewahn et al. 1993; Odewahn & Aldering 1995). We assume a completeness of 85% down to 19.4 $B_{\rm APS}$ as recovered by Odewahn & Aldering (1995) from a comparison with a previous photometric catalog of Coma. In particular, we assume the same level of incompleteness for all magnitudes down to $B_j = 19.4$; this seems true at least for $B_{\rm APS} > 15$ (cf. Fig. 11 of Odewahn et al. 1993).

For each system of A-CL and A-PS we select galaxies with magnitudes $B_{\rm APS} < 19.4$ within circular regions with a radius equal to $R_{\rm vir}$ and a center as chosen in § 3.1.1 for poor systems, or computed by G00 for clusters. Since the APS catalog is still in progress, before including a system in our study we have checked by visual inspection that the photometric data fully cover the selected system region.

3.2.2. *Magnitude Conversion and Correction*

In order to homogenize the photometry coming from the two catalogs, as well as for comparison with results by G00, we convert $B_{\rm APS}$ magnitudes into the B_j band. We consider the 27 systems for which both photometries are available: 22 A-CLs in common with C-CLs of G00, and five PSs. On the base of similar positions, with a maximum distance of 0.′1, we select 4845 system galaxies having magnitudes in

TABLE 2
RESULTS OF DYNAMICAL ANALYSIS

Name (1)	N_f (2)	N_m (3)	V (km s^{-1}) (4)	σ_v (km s^{-1}) (5)	$R_{\rm vir}$ (h^{-1} Mpc) (6)	N (7)	$R_{\rm PV}$[a] (h^{-1} Mpc) (8)	T (9)	M ($h^{-1}\,10^{14}\,M_\odot$) (10)
S49-145	29	10	6812	371^{+57}_{-72}	0.74	4	(0.55± 0.14)	...	$0.66^{+.26}_{-.31}$
S49-142	20	5	6299	122^{+140}_{-140}	0.24	3	(0.18± 0.05)	...	$0.02^{+.05}_{-.05}$
N45-384	26	14	7833	232^{+50}_{-82}	0.46	5	(0.35± 0.09)	...	$0.16^{+.08}_{-.12}$
N34-172	17	9	6007	302^{+89}_{-82}	0.60	6	(0.45± 0.11)	...	$0.36^{+.23}_{-.21}$
N56-393	24	5	6663	311^{+174}_{-27}	0.62	4	(0.46± 0.12)	...	$0.39^{+.45}_{-.12}$
N79-278	40	17	8983	287^{+37}_{-59}	0.57	12	0.25± 0.06	C	$0.19^{+.07}_{-.09}$
N67-312	33	16	6036	131^{+9}_{-67}	0.26	3	(0.19± 0.05)	...	$0.03^{+.01}_{-.03}$
N56-371	53	8	8130	319^{+20}_{-101}	0.64	4	(0.47± 0.12)	...	$0.42^{+.12}_{-.29}$
N79-280	17	10	9390	87^{+10}_{-80}	0.17	1	(0.13± 0.03)	...	$0.01^{+.00}_{-.02}$
N56-392	174	12	7995	172^{+15}_{-95}	0.34	8	0.21± 0.07	A	$0.04^{+.01}_{-.04}$
N79-298	46	7	4478	152^{+47}_{-141}	0.30	6	(0.23± 0.06)	...	$0.05^{+.03}_{-.09}$
N79-299B	26	22	6920	364^{+46}_{-54}	0.73	15	0.58± 0.14	A	$0.47^{+.16}_{-.18}$
N67-335	40	27	5922	515^{+104}_{-87}	1.03	26	0.71± 0.11	A	$1.14^{+.49}_{-.42}$
N79-299A	26	22	6910	391^{+40}_{-60}	0.78	12	0.47± 0.14	...	$0.63^{+.22}_{-.27}$
N79-283	52	24	7970	360^{+84}_{-48}	0.72	18	0.55± 0.13	B	$0.62^{+.32}_{-.22}$
N79-292	116	34	7290	318^{+88}_{-76}	0.64	7	0.48± 0.09	A	$0.29^{+.17}_{-.15}$
N67-333	20	10	14176	489^{+102}_{-47}	0.98	8	0.37± 0.11	A	$0.53^{+.28}_{-.19}$
N67-323	15	6	9212	79^{+43}_{-51}	0.16	2	(0.12± 0.03)	...	$0.01^{+.01}_{-.01}$
N67-317	35	5	7021	223^{+253}_{-253}	0.45	1	(0.33± 0.08)	...	$0.14^{+.33}_{-.33}$
N79-270	9	5	6746	130^{+73}_{-70}	0.26	3	(0.19± 0.05)	...	$0.03^{+.03}_{-.03}$
N79-296	33	20	6779	388^{+69}_{-62}	0.78	11	0.78± 0.18	...	$1.03^{+.43}_{-.40}$
N67-329	13	11	6842	176^{+24}_{-94}	0.35	5	(0.26± 0.07)	...	$0.07^{+.03}_{-.08}$
N79-297	11	5	8730	206^{+76}_{-136}	0.41	2	(0.31± 0.08)	...	$0.11^{+.09}_{-.15}$
N79-276	36	6	11059	540^{+148}_{-70}	1.08	5	(0.80± 0.20)	...	$2.04^{+1.23}_{-.74}$
N67-336	71	25	5843	270^{+65}_{-57}	0.54	20	0.45± 0.06	C	$0.31^{+.15}_{-.14}$
N67-325	8	6	5184	265^{+56}_{-226}	0.53	4	(0.39± 0.10)	...	$0.24^{+.12}_{-.42}$
N67-326	146	33	4532	256^{+26}_{-50}	0.51	11	0.48± 0.13	...	$0.27^{+.09}_{-.13}$
N67-309	16	6	8057	340^{+108}_{-33}	0.68	4	(0.51± 0.13)	...	$0.51^{+.35}_{-.16}$
N56-394	49	23	8586	296^{+35}_{-59}	0.59	14	0.72± 0.10	...	$0.55^{+.15}_{-.23}$
N56-395	27	20	8137	477^{+82}_{-61}	0.95	16	0.67± 0.18	C	$1.44^{+.62}_{-.53}$
N56-381	16	10	8950	259^{+53}_{-79}	0.52	4	(0.39± 0.10)	...	$0.23^{+.11}_{-.15}$
N45-381	50	7	11198	150^{+91}_{-91}	0.30	1	(0.22± 0.06)	...	$0.04^{+.05}_{-.05}$
N45-363	26	7	10995	449^{+146}_{-81}	0.90	7	(0.67± 0.17)	...	$1.17^{+.82}_{-.52}$
N45-389	24	22	9522	656^{+75}_{-84}	1.31	20	1.18± 0.19	B	$4.43^{+1.25}_{-1.35}$
N34-171	13	5	5484	215^{+79}_{-75}	0.43	2	(0.32± 0.08)	...	$0.13^{+.10}_{-.10}$
N34-175	12	6	8894	550^{+212}_{-76}	1.10	5	(0.82± 0.20)	...	$1.50^{+1.22}_{-.56}$
NGC 533	99	36	5518	464^{+54}_{-47}	0.93	36	(0.69± 0.17)	A	$1.30^{+.44}_{-.42}$
HCG 42	106	22	3719	211^{+22}_{-43}	0.42	17	0.32± 0.06	B	$0.13^{+.04}_{-.06}$
NGC 4325	68	18	7468	265^{+36}_{-40}	0.53	16	0.50± 0.10	C	$0.31^{+.10}_{-.11}$
HCG 62	106	46	4307	396^{+57}_{-55}	0.79	46	(0.59± 0.15)	B	$0.87^{+.33}_{-.33}$
NGC 5129	85	33	6938	294^{+33}_{-38}	0.59	26	0.56± 0.06	C	$0.42^{+.11}_{-.12}$
NGC 491	104	6	3987	92^{+70}_{-38}	0.18	4	(0.14± 0.03)	...	$0.01^{+.02}_{-.01}$
NGC 664	67	6	5489	148^{+90}_{-79}	0.30	4	(0.22± 0.06)	...	$0.04^{+.05}_{-.05}$

[a] Values in parentheses are those computed through the alternative estimate by using the typical galaxy distribution (see text).

both catalogs (note that for this analysis we consider somewhat larger areas). We fit B_j versus $B_{\rm APS}$ magnitudes by using the unweighted bisecting procedure (Isobe et al. 1990) for each of the 27 systems; cf. Figure 3, where we show $B_{\rm APS} - B_j$ versus $B_{\rm APS}$ magnitudes for the sake of clarity.

We verify that slopes (and intercepts) of all straight lines can be derived from only one parent value, according to the Homogeneity test (or Variance-ratio test, cf. e.g., Guest 1961), and combine together data of all 27 systems. Figure 4 shows the cumulative relation between the two magnitude bands and the corresponding quadratic fit (via the MINUIT subroutine of CERN Libraries):

$$B_{\rm APS} - B_j = 0.23 + 0.19 \times B_{\rm APS} - 1.02 \times 10^2 \times B_{\rm APS}^2 , \quad (5)$$

performed by using the 1021 galaxies with $B_{\rm APS} < 18$ mag in order to avoid the bias on the difference $(B_{\rm APS} - B_j)$ caused by the limit in B_j.

After having homogeneized all magnitudes to COSMOS B_j, following G00 we apply the correction of Lumsden et al. (1997) to convert COSMOS B_j magnitudes to the CCD-based magnitude scale. This correction is consistent with our choice to use the luminosity function and counts by Lumsden et al. (1997). Finally, we correct each galaxy magnitude for (1) Galactic absorption by assuming the absorption in the blue band as given by de Vaucouleurs et al. (1991) in the region of each system, and (2) K-dimming by assuming that all galaxies lie at the average system redshift (Colless 1989). The correction for internal galactic absorp-

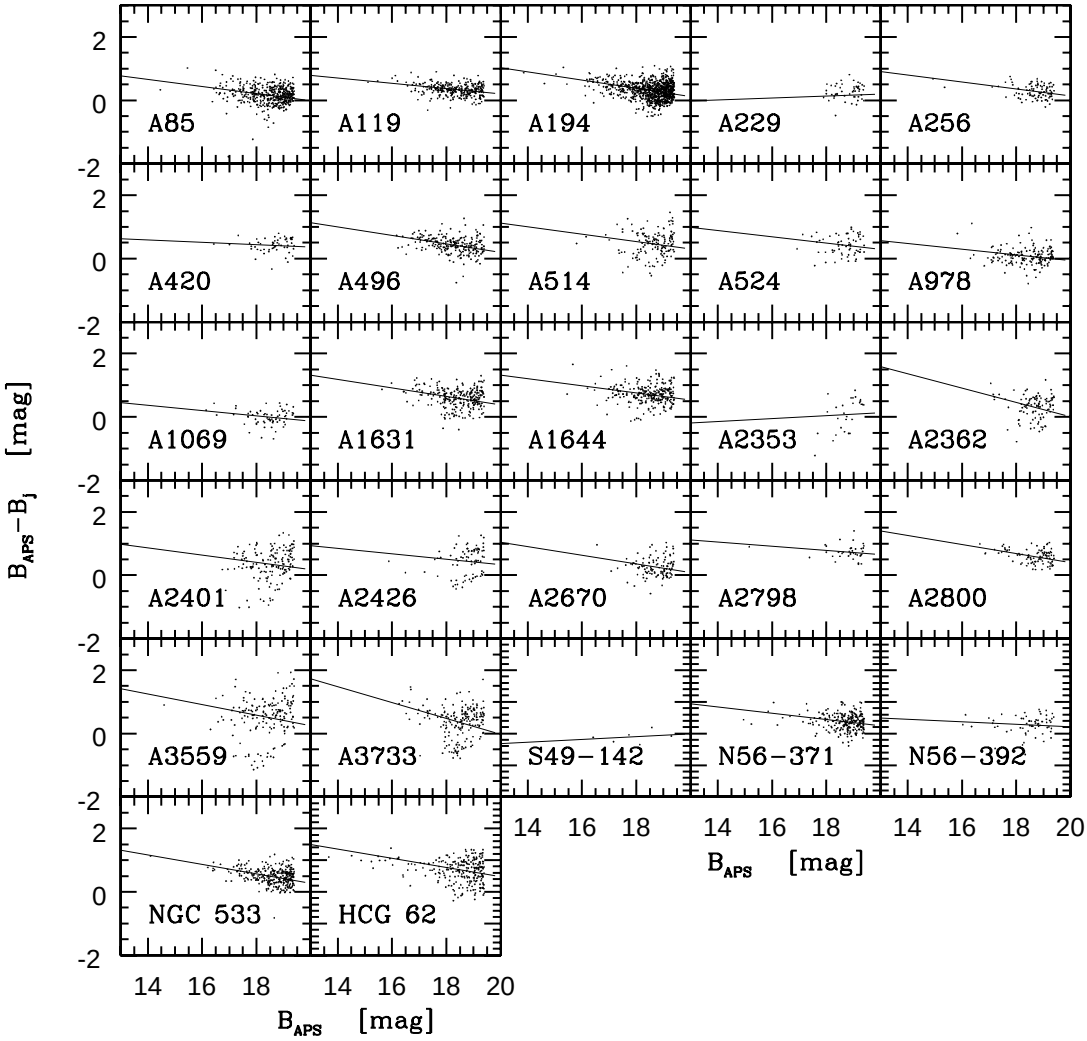

FIG. 3.—Comparison of magnitudes from COSMOS and APS catalogs for the galaxies of the 27 systems having both photometries available. The faint lines represent the result of the (bisecting) fitting of B_j vs. $B_{\rm APS}$.

tion will be taken into account at the end of the procedure to estimate luminosities.

3.2.3. *Luminosities from COSMOS and APS*

For all C-PSs, A-PSs, and A-CLs we compute total luminosities within $R_{\rm vir}$ following the procedure already outlined for C-CLs by G00 who used COSMOS. Having already homogeneized the original APS magnitudes to the B_j band, the whole procedure is the same except for the value of the magnitude incompleteness in the catalogs (cf. point 2 below). Here we give a short summary of the procedure.

1. We compute observed system luminosities, $L_{B_j,\rm obs}$, obtained by summing the individual absolute luminosities of all galaxies and assuming $B_{j,\odot} = 5.33$ (i.e., $B_\odot = 5.48$ and using the conversion to B_j by Kron 1978).

2. For samples from the COSMOS (or APS) catalog we correct for 91% (or 85%) incompleteness, obtaining $L_{B_j,\rm compl} = L_{B_j,\rm obs}/0.91$. (or $L_{B_j,\rm compl} = L_{B_j,\rm obs}/0.85$), and the same correction is also applied to number counts.

3. We subtract the average fore/background luminosity obtained from the mean field B_j counts by Lumsden et al. (1997) using the EDSGC (cf. their Fig. 2, corrected for 95% completeness): $L_{B_j,\rm corr} = L_{B_j,\rm compl} - L_{B_j,\rm meanfield}$. We correct counts in a similar way. The median correction is 29%.

4. We include the luminosity of faint galaxies below the magnitude completeness limit $L_{B_j,\rm extr} = L_{B_j,\rm corr} + L_{B_j,\rm faint}$, where $L_{B_j,\rm faint}$ is obtained by extrapolating the usual Schechter (1976) form for the cluster luminosity function (with $M^*_{Bj} = -20.16$ for the characteristic magnitude and $\alpha = -1.22$ for the slope as determined by Lumsden et al. 1997), normalized by using the observed (corrected) galaxy number counts for $-21 \le M_{B_j} \le -18$ (cf. eqs. [1] and [2] of G00). The median correction is 5%.

5. The final luminosity estimate of galaxy systems, L_{B_j}, takes into account the internal galactic absorption by adopting a correction of $\Delta B_j = 0.1$ mag. On account of to this correction, the luminosity increases by about 10%.

$L_{B_j,c,\rm COSMOS}$ and $L_{B_j,c,\rm APS}$ denote luminosities computed for the two catalogs.

The above method for the fore/background correction does not take into account the local field-to-field count variations, which lead to random errors. Since this correction is the largest one in our procedure, it is worthwhile considering an alternative procedure, too. Following G00, we also consider the method recently used by Rauzy, Adami, &

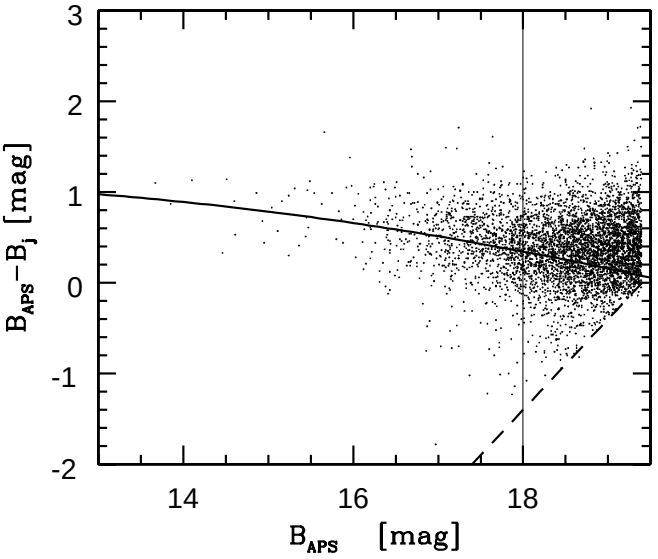

FIG. 4.—Relationship between COSMOS and APS magnitudes obtained by combining data for all 27 systems shown in Fig. 3. The solid line represents the best quadratic fit, which is performed on the data with $B_{APS} < 18$ mag to avoid the bias on the difference ($B_{APS} - B_j$) caused by the limit in B_j, as shown by the dashed line.

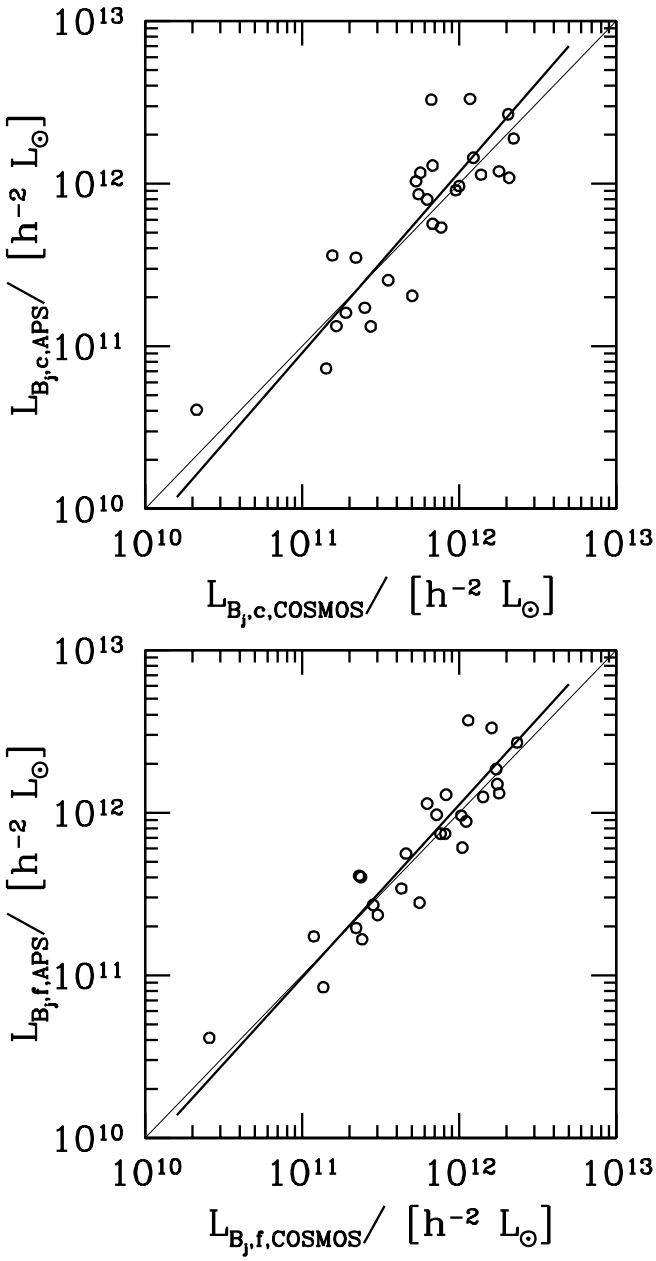

FIG. 5.—Comparison between the luminosities derived from the APS catalog with those derived from the COSMOS catalog for the 27 galaxy systems with both photometries available, and for both the two alternative estimates of the fore/background correction: by using the mean counts (*top panel*) or the member fraction (*bottom panel*). The solid lines represent the (bisecting) fitting to be compared to the one-to-one relation (*the faint line*).

Mazure (1998) to take into account the very local field, i.e., the presence of a nearby group along the system LOS. This method is based on the idea that having redshifts for all galaxies would allow an unambiguous determination of the membership and thus the solution of the fore/background correction. Rauzy et al. suggested correcting cluster luminosity (and counts) by assuming that the fraction of members of the examined photometric sample corresponds, for luminosity and number, to that computed on a corresponding sample of galaxies all having redshift ($L_{B_j,\mathrm{corr}} = L_{B_j,\mathrm{obs}} \times f_L$ and $N_{\mathrm{corr}} = N_{\mathrm{obs}} \times f_N$). The drawback of this method is obviously that the estimated member fraction computed in the redshift sample depends on the magnitude limit and the extension of the sampled region. Here we use the redshift samples analyzed in § 3.1 for poor systems and those analyzed by G98 for clusters in order to compute f_N and f_L within R_{vir}. The fraction f_N is directly recovered by comparing the number of member galaxies with those in the field. As for clusters, following G00, we compute f_L when original redshift samples have available magnitudes, or assume that $f_L = f_N$ when luminosities are not directly available (since $f_L \sim f_N$). As for poor systems, we compute f_L after assigning to galaxies of redshift samples the corresponding magnitudes taken from the photometric samples (here $f_L > f_N$ for a typical factor of 30%); when less than five galaxies are available we use the median values $f_L = 0.8$ and $f_N = 0.6$ as computed on all better sampled poor systems. $L_{B_j,f,\mathrm{COSMOS}}$ and $L_{B_j,f,\mathrm{APS}}$ denote our alternative luminosity estimates.

Table 3 gives the results of luminosity computation, reporting the results of G00 too, for both clusters and poor systems (CL+PS sample, 162 systems), which make up a very homogeneous sample for both mass and luminosity estimates. We list the system name (col. [1]); the adopted system center (col. [2]); R_{vir}, the virial radius (col. [3]); N_{APS}, the number of galaxies within R_{vir}, used to compute $L_{Bj,c,\mathrm{APS}}$ and $L_{Bj,f,\mathrm{APS}}$, the two alternative APS luminosities based on two procedures for the fore/background correction (cols. [4], and [5], respectively); N_{COSMOS}, the number of galaxies within R_{vir}, used to compute $L_{Bj,c,\mathrm{COSMOS}}$ and $L_{Bj,f,\mathrm{COSMOS}}$, the two alternative COSMOS luminosities (cols. [6], and [7], respectively).

Figure 5 compares the luminosities derived from the COSMOS catalog with those derived from the APS catalog for the 27 systems having both photometries available. For both the two alternative estimates (Figs. 5*a* and 5*b*) the fitted straight lines in the logarithmic plane are consistent with the one-to-one relation within 1 σ (using the unweighted bisecting fit; cf. Isobe et al. 1990). This

TABLE 3

LUMINOSITY ESTIMATES

Name (1)	Center α(2000)-δ(2000) (2)	$R_{\rm vir}$ (h^{-1} Mpc) (3)	$N_{\rm APS}$ (4)	$L_{B_j,{\rm APS}}$[a] (10^{11} h^{-2} $L_{B_j,\odot}$) (5)	$N_{\rm COSMOS}$ (6)	$L_{B_j,{\rm COSMOS}}$[a,b] (10^{11} h^{-2} $L_{B_j,\odot}$) (7)
A85	004140.6−091833	1.94	462	26.75, 26.93	403	20.55, 23.41
A119	005617.9−011528	1.36	280	11.36, 14.99	370	13.78, 17.48
A193	012505.4+084157	1.45	200	6.64, 10.29	...	..., ...
A194	012552.6−012008	0.68	150	1.73, 2.35	218	2.50, 3.03
A229	013914.5−033803	1.01	35	5.66, 7.41	50	6.80, 8.15
A256	014804.5−035429	1.09	56	9.68, 7.42	85	10.00, 7.61
A262	015246.7+360856	1.05	1307	15.12, 14.12	...	..., ...
A295	020211.8−010603	0.72	...	..., ...	137	5.94, 5.81
A400	025740.7+060048	1.20	351	6.03, 6.61	...	..., ...
A420	030916.8−113226	0.72	25	1.33, 1.66	45	2.73, 2.41
A458	034605.4−242040	1.47	...	..., ...	114	12.44, 17.82
A496	043331.8−131703	1.37	323	5.38, 8.81	526	7.68, 11.09
A514	044830.1−203330	1.76	214	33.19, 33.26	294	11.72, 16.10
A524	045743.2−194345	0.50	27	3.50, 1.73	33	2.20, 1.19
A978	102028.5−063050	1.07	165	8.60, 9.72	161	5.51, 7.18
A999	102325.4+124958	0.56	61	3.71, 3.12	...	..., ...
A1060	103631.2−272935	1.22	...	..., ...	3678	8.80, 11.75
A1069	103937.0−083121	0.72	67	7.98, 5.60	72	6.25, 4.59
A1142	110154.8+101835	0.97	133	3.32, 4.43	...	..., ...
A1146	110116.4−224413	1.86	...	..., ...	148	38.51, 43.15
A1185	111044.4+284145	1.07	380	6.20, 7.68	...	..., ...
A1228	112151.2+342201	0.34	35	2.17, 1.47	...	..., ...
A1314	113428.0+490243	0.55	97	4.27, 4.56	...	..., ...
A1631	125258.2−152111	1.40	357	18.95, 12.49	511	22.25, 14.21
A1644	125723.3−172448	1.52	328	11.92, 13.15	524	17.91, 17.97
A1656	125937.2+275712	1.64	1136	21.36, 26.80	...	..., ...
A1795	134849.3+263347	1.67	239	14.08, 19.52	...	..., ...
A1809	135256.0+050760	1.53	144	11.09, 18.77	...	..., ...
A1983	145258.1+164129	0.99	233	5.97, 7.44	...	..., ...
A1991	145432.6+183735	1.26	158	7.55, 10.84	...	..., ...
A2029	151056.7+054500	2.33	504	49.67, 65.10	...	..., ...
A2040	151246.4+072517	0.92	158	8.01, 7.87	...	..., ...
A2048	151516.9+042229	1.33	109	15.05, 15.90	...	..., ...
A2079	152745.1+285508	1.34	172	12.12, 13.89	...	..., ...
A2092	153323.2+310856	1.07	106	7.01, 6.77	...	..., ...
A2107	153941.1+214843	1.24	242	7.43, 9.53	...	..., ...
A2124	154447.2+360440	1.76	286	31.60, 40.53	...	..., ...
A2142	155819.8+271435	2.26	275	29.36, 44.31	...	..., ...
A2151	160510.5+174522	1.50	626	15.44, 18.97	...	..., ...
A2197	162946.7+405036	1.22	546	11.48, 15.02	...	..., ...
A2199	162843.0+393043	1.60	797	19.75, 25.61	...	..., ...
A2353	213422.3−013507	1.19	36	32.84, 36.90	47	6.65, 11.41
A2362	213901.3−141911	0.66	54	3.62, 4.09	55	1.56, 2.30
A2401	215821.1−200557	0.79	165	11.68, 11.38	132	5.65, 6.26
A2426	221411.9−101103	0.66	71	12.95, 4.01	62	6.77, 2.36
A2500	225351.8−253103	0.95	...	..., ...	63	3.90, 2.64
A2554	231212.7−213050	1.68	...	..., ...	181	24.52, 26.66
A2569	231757.8−124635	0.98	...	..., ...	79	6.34, 8.71
A2589	232401.4+164834	0.94	106	2.90, 4.18	...	..., ...
A2634	233828.4+270133	1.40	507	20.90, 24.40	...	..., ...
A2644	234035.7−000350	0.36	...	..., ...	15	0.68, 0.48
A2670	235414.6−102505	1.70	201	14.42, 18.53	245	12.33, 17.24
A2715	000245.2−343932	0.93	...	..., ...	46	6.25, 4.20
A2717	000310.8−355557	1.08	...	..., ...	172	3.1, 4.78
A2721	000607.9−344302	1.61	...	..., ...	157	19.71, 27.65
A2734	001126.6−285018	1.26	...	..., ...	184	4.64, 8.12
A2755	001736.9−351059	1.54	...	..., ...	197	15.88, 15.36
A2798	003733.1−283205	1.42	37	10.87, 6.10	108	20.84, 10.48
A2799	003723.1−390750	0.84	...	..., ...	95	3.80, 5.37
A2800	003804.2−250610	0.81	42	2.55, 3.42	70	3.53, 4.29
A2877	010948.3−455702	1.77	...	..., ...	1379	10.94, 16.55
A2911	012604.0−375609	1.09	...	..., ...	106	11.47, 6.02
A3093	031057.5−472426	0.88	...	..., ...	71	4.62, 5.28

TABLE 3—*Continued*

Name (1)	Center α(2000)-δ(2000) (2)	$R_{\rm vir}$ (h^{-1} Mpc) (3)	$N_{\rm APS}$ (4)	$L_{B_j,{\rm APS}}$[a] (10^{11} h^{-2} $L_{B_j,\odot}$) (5)	$N_{\rm COSMOS}$ (6)	$L_{B_j,{\rm COSMOS}}$[a,b] (10^{11} h^{-2} $L_{B_j,\odot}$) (7)
A3094	031140.7−265908	1.31	...	..., ...	223	10.55, 12.30
A3111	031738.6−454656	0.32	...	..., ...	30	3.10, 0.98
A3122	032210.7−411905	1.55	...	..., ...	223	4.63, 9.60
A3126	032833.0−554241	2.11	...	..., ...	281	10.98, 24.02
A3128	033052.6−523023	1.58	...	..., ...	434	19.26, 21.86
A3142	033644.0−394616	1.47	...	..., ...	132	12.55, 9.99
A3151	034034.4−284043	0.47	...	..., ...	57	4.10, 1.56
A3158	034259.7−533759	1.95	...	..., ...	669	19.38, 26.03
A3194	035908.8−301044	1.61	...	..., ...	203	16.99, 26.23
A3223	040809.7−310248	1.29	...	..., ...	263	9.39, 10.83
A3266	043046.8−613408	2.21	...	..., ...	780	24.76, 28.87
A3334	051749.1−583325	1.39	...	..., ...	96	6.68, 11.86
A3354	053442.5−284046	0.72	...	..., ...	102	8.23, 5.43
A3360	054007.3−432358	1.67	...	..., ...	140	9.05, 17.06
A3376	060215.5−395625	1.38	...	..., ...	288	5.45, 8.95
A3381	060957.0−333320	0.59	...	..., ...	126	4.61, 2.01
A3391	062617.6−534143	1.33	...	..., ...	278	16.26, 16.35
A3395	062735.6−542629	1.70	...	..., ...	496	16.04, 15.87
A3528N	125426.7−290017	0.92	229	14.14, 8.85	...	..., ...
A3532	125715.3−302105	1.48	...	..., ...	463	18.92, 17.32
A3556	132418.2−314220	1.28	...	..., ...	409	16.22, 15.02
A3558	132755.5−312921	1.95	...	..., ...	1151	50.30, 55.51
A3559	133011.5−293400	0.91	186	9.10, 9.60	215	9.52, 10.32
A3571	134720.8−325210	2.09	...	..., ...	1746	35.97, 45.65
A3574	134849.3−302735	0.98	...	..., ...	1303	8.56, 9.25
A3651	195226.3−550815	1.25	...	..., ...	348	21.34, 19.65
A3667	201226.5−564840	1.94	...	..., ...	882	40.78, 40.10
A3693	203420.5−343311	0.96	...	..., ...	89	8.31, 4.59
A3695	203445.0−354809	1.56	...	..., ...	214	20.65, 26.62
A3705	204210.2−351215	1.75	...	..., ...	327	29.61, 32.44
A3733	210135.2−280232	1.22	342	10.34, 12.89	301	5.30, 8.27
A3744	210723.8−252558	1.02	...	..., ...	340	6.55, 7.76
A3809	214715.8−435523	0.96	...	..., ...	162	5.78, 7.14
A3822	215414.8−575103	1.62	...	..., ...	545	36.26, 33.83
A3825	215819.6−601828	1.40	...	..., ...	298	16.96, 16.56
A3879	222759.3−685547	0.80	...	..., ...	81	4.86, 5.15
A3880	222751.7−303419	1.65	...	..., ...	365	14.66, 19.75
A3921	225003.3−642351	0.98	...	..., ...	117	12.05, 13.37
A4008	233020.5−391538	0.85	...	..., ...	126	4.71, 5.34
A4010	233132.1−363010	1.25	...	..., ...	102	8.67, 10.56
A4053	235442.6−274115	1.23	...	..., ...	136	6.16, 4.60
A4067	235856.9−603730	1.00	...	..., ...	84	8.11, 8.74
S84	004925.3−293051	0.66	...	..., ...	50	6.81, 5.08
S373	033603.9−351343	0.62	...	..., ...	4150	1.28, 3.68
S463	042911.7−535013	1.22	...	..., ...	416	15.80, 16.22
S721	130604.4−373704	1.38	...	..., ...	463	11.36, 12.25
S753	140316.0−340318	1.07	...	..., ...	1653	5.10, 5.65
S805	185246.3−631441	1.08	...	..., ...	2133	6.28, 7.59
S987	220154.8−222433	1.35	...	..., ...	206	21.45, 25.42
S1157/C67	235139.8−342714	1.16	...	..., ...	191	8.87, 5.36
AWM4	160455.3+235627	0.24	26	1.62, 0.75	...	..., ...
CL 2335-26	233753.1+271047	1.20	51	58.34, 51.83	...	..., ...
DC0003-50	000604.6−503842	0.70	...	..., ...	146	3.17, 3.96
Eridanus	034014.6−183725	0.53	...	..., ...	1536	0.52, 0.96
MKW1	100044.2−025741	0.45	...	..., ...	185	1.51, 1.82
MKW6A	141439.7+030753	0.55	80	1.38, 2.04	...	..., ...
S49-145	020734.9+020814	0.74	...	..., ...	279	3.47, (3.68)
S49-142	032044.7−010215	0.24	21	0.41, (0.41)	16	0.21, (0.26)
N45-384	092751.8+295956	0.46	149	1.57, 0.90	...	..., ...
N34-172	100032.1−025727	0.60	158	1.05, 1.43	...	..., ...
N56-393	101352.0+384007	0.62	116	1.50, (1.87)	...	..., ...
N79-278	113754.4+215823	0.57	63	1.24, 1.60	...	..., ...
N67-312	114204.6+101820	0.26	53	0.75, (0.71)	...	..., ...
N56-371	114503.5−013938	0.64	162	1.61, (1.95)	246	1.90, (2.21)

TABLE 3—*Continued*

Name (1)	Center $\alpha(2000)$-$\delta(2000)$ (2)	$R_{\rm vir}$ (h^{-1} Mpc) (3)	$N_{\rm APS}$ (4)	$L_{B_j,{\rm APS}}$[a] ($10^{11}\ h^{-2}\ L_{B_j,\odot}$) (5)	$N_{\rm COSMOS}$ (6)	$L_{B_j,{\rm COSMOS}}$[a,b] ($10^{11}\ h^{-2}\ L_{B_j,\odot}$) (7)
N79-280	114618.5+330919	0.17	25	1.07, (0.89)	...	..., ...
N56-392	114938.9−033135	0.34	31	0.73, 0.84	65	1.42, 1.36
N79-298	115752.3+251018	0.30	71	0.35, (0.42)	...	..., ...
N79-299B	120409.5+201318	0.73	234	3.13, 3.00	...	..., ...
N67-335	120421.7+015019	1.03	490	1.41, 1.60	...	..., ...
N79-299A	120551.2+203219	0.78	200	2.77, 2.86	...	..., ...
N79-283	121954.8+282521	0.72	183	6.99, 2.09	...	..., ...
N79-292	122414.7+092024	0.64	80	0.36, 0.43	...	..., ...
N67-333	130425.3+075454	0.98	110	2.63, 2.49	...	..., ...
N67-323	130526.5+533356	0.16	11	0.48, (0.42)	...	..., ...
N67-317	131349.0+065709	0.45	64	0.42, (0.63)	...	..., ...
N79-270	131719.3+203711	0.26	26	0.41, (0.43)	...	..., ...
N79-296	132922.3+114731	0.78	289	2.72, 2.08	...	..., ...
N67-329	133236.4+072036	0.35	39	0.76, (0.81)	...	..., ...
N79-297	135524.7+250320	0.41	65	1.75, (1.67)	...	..., ...
N79-276	135622.3+283123	1.08	206	1.92, 1.78	...	..., ...
N67-336	140304.0+092635	0.54	159	2.99, 2.91	...	..., ...
N67-325	140958.5+173251	0.53	199	1.76, (2.00)	...	..., ...
N67-326	142814.1+255038	0.51	199	0.67, (0.97)	...	..., ...
N67-309	142831.6+112238	0.68	119	1.68, (2.08)	...	..., ...
N56-394	143400.9+034453	0.59	109	1.41, 1.73	...	..., ...
N56-395	144043.2+032712	0.95	302	1.96, 3.06	...	..., ...
N56-381	144700.4+113529	0.52	62	0.31, (0.64)	...	..., ...
N45-381	151311.6+042850	0.30	41	1.60, (1.40)	...	..., ...
N45-363	155746.9+161627	0.90	178	4.52, 2.67	...	..., ...
N45-389	161739.2+350545	1.31	408	6.46, 9.40	...	..., ...
N34-171	164135.4+575021	0.43	97	0.35, (0.57)	...	..., ...
N34-175	171521.4+572243	1.10	976	12.18, (12.11)	...	..., ...
NGC 533	012529.9+014537	0.93	311	1.33, 2.71	597	1.65, 2.83
HCG 42	100018.6−193860	0.42	...	..., ...	554	2.29, 2.40
NGC 4325	122304.6+103352	0.53	57	0.44, 0.76	...	..., ...
HCG 62	125305.1−091247	0.79	449	2.04, 2.79	978	5.03, 5.59
NGC 5129	132425.2+135455	0.59	129	1.79, 2.27	...	..., ...
NGC 491	012102.7−340358	0.18	...	..., ...	51	0.34, (0.32)
NGC 664	014314.4+041319	0.30	27	0.23, (0.32)	...	..., ...

NOTE.—Table 3 is also available in machine-readable form in the electronic edition of the *Astrophysical Journal*.

[a] Both alternative estimates of luminosity are given ($L_{Bj,c}$, $L_{Bj,f}$). Values in parentheses are $L_{Bj,f}$, which are not based on individual member fraction estimates, but on median values.

[b] We report values computed by G00 for clusters (C-CL sample), too.

fair agreement supports the homogeneity of our luminosity estimates, although recovered from two different photometric catalogs, and justify their combination. When both APS and COSMOS luminosities are available, we consider their average.

Figure 6 compares the two alternative luminosity estimates $L_{Bj,c}$ and $L_{Bj,f}$ for all 119 CLs and those 22 PSs for which we compute individual member fractions. The (bisecting) fit is consistent with the one-to-one relation, within 2 σ, indicating that any systematic bias connected to the fore/background correction should not seriously pollute our analysis. More particularly, Figure 6 shows no systematic overestimate of $L_{B_j,c}$ with respect to $L_{B_j,f}$, as expected when subtracting the mean field luminosity density from cluster regions, when clusters are selected as overdensities in a projected galaxy distribution. This is due to two main reasons. First, systematic foreground/background contamination for nearby clusters is small (e.g., only $\sim$10% for ENACS, Katgert et al. 1996); second, in this study we exclude, a priori, clusters showing two significant peaks in the velocity distribution, which are the most contaminated clusters (cf. §§ 2.1 and 3.1.1). The comparison in Figure 6 suggests that the majority of clusters has $L_{B_j,f} > L_{B_j,c}$, although for a small amount ($L_{B_j,f}/L_{B_j,c} = 1.1$, median value), probably because that the member fractions we determine in the redshift samples are slightly larger than the appropriate ones for the (deeper) magnitude samples. The distribution of the scatter is not symmetric with respect the one-to-one relation, thus suggesting competition between two different sources of errors. This supports the use, in our final results, of the average of the two estimates.

As for the error estimates, the scatter in the $L_{Bj,c}$-$L_{Bj,f}$ relation ($\sim$25%) provides an estimate of the random errors due to the variations of local field, i.e., to the procedure adopted, while the scatter in the COSMOS-APS comparison ($\sim$40% and $\sim$30% in the two cases) also gives an idea of the random errors connected with the photometry of the catalogs. By adding in the quadrature the two sources of errors, we assume that the error on each individual luminosity is $\lesssim$50%.

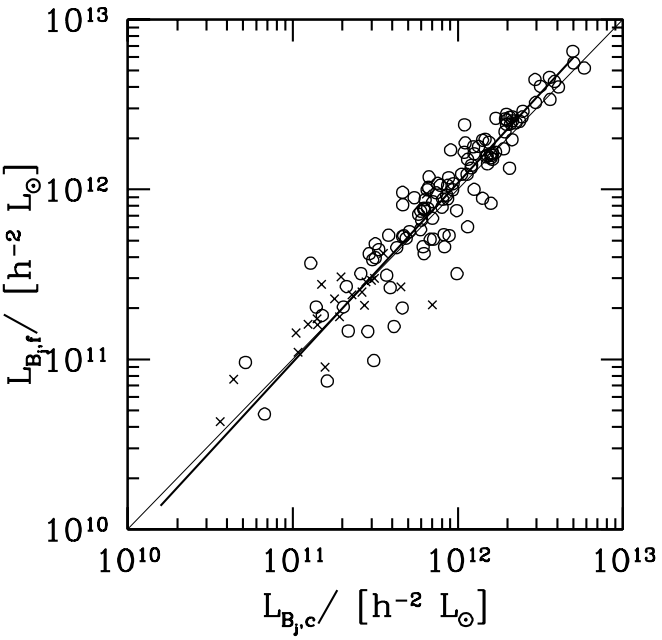

FIG. 6.—Comparison between the two alternative luminosity estimates based on the two different fore/background corrections: by using the mean counts ($L_{B_j,c}$) or the member fraction ($L_{B_j,f}$). Circles and crosses indicate clusters and poor systems, respectively. The solid line represents the (bisecting) fitting to be compared to the one-to-one relation (*the faint line*).

3.3. *Mass and Luminosity for NOG Groups*

Here we compute mass and luminosity for each group of NOG group catalogs, PG and HG.

The observational determination of group M/L encounters several additional problems. These problems arise in the estimate of mass and are mainly due to the poor number of group members and to the uncertainties in the dynamical stage. In fact, although group cores are close to virialization or virialized (ZM98; Zabludoff & Mulchaey 1998b), the sampling area of groups identified in three-dimensional galaxy catalogs is well outside their likely virialized region (e.g., Girardi & Giuricin 2000, hereafter GG00; Carlberg et al. 2001a). Also older works indicated that, by considering their whole sampled region, these groups cannot be considered virialized systems, but rather described as being in a phase of collapse (e.g., Giuricin et al. 1988; Diaferio et al. 1993; Mamon 1994). The small number of galaxies prevents us from applying refined analyses such as those used for clusters and well-sampled groups, e.g., the member selection or the analysis of velocity dispersion profiles (cf. G98 and references therein; ZM98; Mahdavi et al. 1999). Above all, the small number of galaxies prevent us from working in smaller, quasi-virialized, group regions.

Therefore, for computing group masses we could not apply the procedure used in § 3.1, but we rather use the procedure recently adopted by GG00. Here we summarize the main steps of this procedure.

First of all, we do not perform any procedure of member selection, but we rely on the group membership as assigned by Giuricin et al. (2000). The comparison of the results coming from the two catalogs of groups identified in the same galaxy catalog, but with two different member assignments, will allow us to check a posteriori the effect of the membership procedure.

Then we compute the LOS velocity dispersion, σ_v, and the (projected) radius used in the virial theorem, $R_{\rm PV}$, in the same way as performed in § 3.1; in particular, for each galaxy we assume a typical velocity error of 30 km s^{-1}. The corresponding virial mass is $M_V = 3\pi\sigma_v^2 R_{\rm PV}/(2G)$. When the correction for velocity errors leads to a negative value of σ_v, σ_v and mass are considered null.

To take into account the dynamical state of groups we use the method proposed by Giuricin et al. (1988). This method is based on the classical model of spherical collapse where the initial density fluctuation grows, lagging behind the cosmic expansion when it breaks away from the Hubble flow, and begins to collapse, and the authors used the results of very simple numerical simulations of galaxy systems (Giuricin et al. 1984; the limits of this model are discussed in § 7.1 of GG00). Using the above method, the value of A, which is needed to recover corrected masses as $M_{VC} = (1/2A)M_V$, can be inferred from the estimate of the presently observed crossing time. In particular, the precise value of A depends on the background cosmology: for our reference model we obtain a typical correction of 0% and 30% for PGs and HGs, respectively (cf. GG00 for other examples).

As for the luminosity computation, we gain a great advantage with respect to poor systems in § 3.2. In fact, the NOG catalog is already homogeneized for photometry; the total blue magnitudes, B, are already corrected (for Galactic absorption, K-dimming, and internal absorption); and the known membership avoids the problem of fore/background contamination. Taking into account these differences, we apply a procedure similar to that outlined in § 3.2.3, i.e.: we compute observed group luminosities, $L_{B,\rm obs}$ (assuming $B_\odot = 5.48$), which here refer to the whole sampled region; we correct for 97% NOG incompleteness, obtaining $L_{B,\rm compl}$; we include the luminosity of faint galaxies below the magnitude completeness limit to obtain total luminosity $L_{B,\rm tot}$, with $M_B^* = -19.97$ for the characteristic magnitude and $\alpha = -1.16$ for the slope (Giuricin et al. 2000). The median correction for faint galaxies is less than 1%.

For the two NOG catalogs, PG and HG, as well as some subsamples: PG5 and HG5, PG7 and HG7, i.e., groups having at least five and seven members, respectively, we give median values (and 90% c.l. error bands) for interesting physical quantities. Table 4 lists the sample name (col. [1]); N_G, the number of groups (col. [2]), and the median values for: N_m, the number of member galaxies (col. [2]); $R_{\rm max}$, the group size which is the projected distance of the most distant galaxy from the group center, here computed as the biweight center (col. [4]); σ_v, the LOS velocity dispersion (col. [5]); $R_{\rm PV}$, the projected radius used in the virial theorem (col. [6]); M_V and M_{VC}, the virial mass, before and after the correction for the dynamical status (cols. [7] and [8]); $L_{B,\rm tot}$, the blue luminosity (col. [9]). Both mass and luminosity refer to the whole sampled region.

Typical mass errors are very large and vary with group mass: e.g., we find a median mass error of ~130% on the whole catalogs, and only ~70% for groups with at least five members. Both mass and luminosity could have large systematic errors connected to the algorithm of identification: for instance the typical mass of PG and HG differs for a 60%, while the luminosity seems robust enough.

TABLE 4
RESULTS FOR NOG GROUPS

Cat. (1)	N_G (2)	N_m (3)	$R_{\max}$ (h^{-1} Mpc) (4)	σ_v (km s^{-1}) (5)	$R_{\rm PV}$ (h^{-1} Mpc) (6)	M_V ($10^{13}\,h^{-1}\,M_\odot$) (7)	$M_{\rm CV}$ ($10^{13}\,h^{-1}\,M_\odot$) (8)	$L_{B,\rm tot}$ ($10^{11}\,h^{-2}\,L_{B,\odot}$) (9)
PG	513	4	$0.46^{+0.04}_{-0.04}$	132^{+12}_{-13}	$0.49^{+0.03}_{-0.05}$	$0.81^{+0.17}_{-0.15}$	$0.85^{+0.22}_{-0.17}$	$0.52^{+0.04}_{-0.03}$
PG5 ...	208	7	$0.60^{+0.06}_{-0.03}$	162^{+17}_{-22}	$0.53^{+0.04}_{-0.04}$	$1.49^{+0.33}_{-0.43}$	$1.47^{+0.34}_{-0.23}$	$0.82^{+0.08}_{-0.09}$
PG7 ...	112	10	$0.76^{+0.04}_{-0.09}$	199^{+11}_{-19}	$0.56^{+0.08}_{-0.04}$	$2.44^{+0.73}_{-0.62}$	$2.57^{+0.58}_{-0.68}$	$1.15^{+0.14}_{-0.21}$
HG	475	4	$0.58^{+0.04}_{-0.03}$	84^{+7}_{-6}	$0.60^{+0.05}_{-0.05}$	$0.43^{+0.07}_{-0.12}$	$0.53^{+0.16}_{-0.09}$	$0.52^{+0.04}_{-0.06}$
HG5...	190	7	$0.81^{+0.06}_{-0.07}$	106^{+8}_{-7}	$0.66^{+0.05}_{-0.06}$	$0.78^{+0.22}_{-0.12}$	$1.05^{+0.17}_{-0.27}$	$0.92^{+0.16}_{-0.08}$
HG7...	103	10	$0.98^{+0.13}_{-0.13}$	120^{+11}_{-8}	$0.71^{+0.08}_{-0.08}$	$1.22^{+0.33}_{-0.26}$	$1.57^{+0.48}_{-0.46}$	$1.23^{+0.28}_{-0.13}$

3.4. *NOG Groups versus Other Galaxy Systems*

As for a reliable comparison with clusters analyzed by G00, and other galaxy systems analyzed in §§ 3.1 and 3.2, we should rescale both group mass and luminosity to the region within $R_{\rm vir}$. The paucity of data does not allow us to make an individual correction: we apply a mean correction to all groups by using the procedure outlined by G00.

PGs and HGs are identified by using a number density contrast $(\delta\rho/\rho)_g = 80$ and a luminosity density contrast $(\delta\rho/\rho)_g = 45$, respectively, which are comparable to the matter density contrast, $\delta\rho/\rho$, since the biasing factor $b = (\delta\rho/\rho)_g/(\delta\rho/\rho)$ is roughly one (e.g., from $b = 1/\sigma_8$ and σ_8-value from Eke et al. 1996; Girardi et al. 1998a). These values of $\delta\rho/\rho$ for *PG* and *HG* groups are much smaller than the values of $\sim$350 expected within the virialized region (e.g., Eke et al. 1996).

After assuming that groups have a common radial profile (Fasano et al. 1993), we can roughly estimate the number fraction of members contained in the virialized region. For each of the two catalogs, Figure 7 plots the cumulative distributions of the projected galaxy distances from the group center, combining together data of all groups. To combine the galaxies of all groups we divide each galaxy distance by the projected radius, $R_{\rm PV}$, of its group and then we normalize to the mean $\langle R_{\rm PV}/R_{\max}\rangle$ of the catalog. From Figure 7 one can infer the fraction of the number of galaxies, i.e., the fraction of group luminosity and mass if galaxy number distribution traces luminosity and mass, contained within each radius. We are interested in determining the radius, and the corresponding number fraction, for which one obtains a density enhancement which is large enough to reach the density contrast expected in the virialized region. In the case of PG, the virialization density is obtained within a radius smaller by $\sim$55%, which contains $\sim$73% fewer galaxies; in fact the density in these central regions is $0.73/(0.55^3) \times 80 = \sim 4.4 \times 80 \sim 350$. In the case of HG, similar arguments show that the virialization density is obtained within a radius smaller by $\sim$42%, which contains $\sim$57% fewer galaxies. The direct application of $R_{\rm vir}$ definition (eq. [1]) would give similar small virialization radii: e.g., for PG groups the median value of $\sigma_v \sim 132$ km s^{-1} corresponds to a value of $R_{\rm vir} = 0.26\,h^{-1}$ Mpc to be compared with the sampling area of groups $R_{\max} = 0.46\,h^{-1}$ Mpc, i.e., $\sim$56% smaller (cf. also Carlberg et al. 2001a for CNOC2 groups).

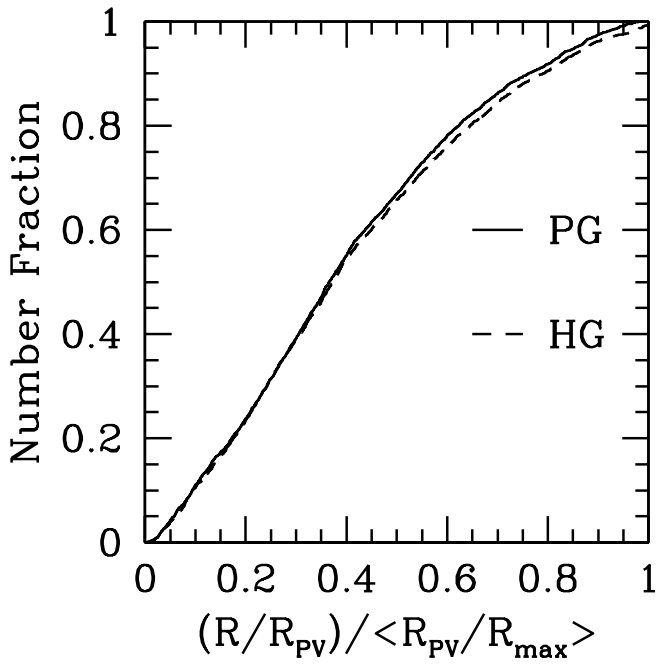

FIG. 7.—For both PG and HG catalogs we show the cumulative distribution of the projected galaxy distances from the group center. To combine the galaxies of all groups we divide each galaxy distance by the projected radius, $R_{\rm PV}$, of its group. Moreover, we also normalize the distances to the median $\langle R_{\rm PV}/R_{\max}\rangle$ of the catalog.

Owing to all uncertainties involved, we consider a similar intermediate correction for all groups of both catalogs and assume these fiducial values for virialized regions: $R_{\rm vir} = 0.5 \times R_{\max}$, $M = 0.65 \times M_{VC}$, and $L_B = 0.65 \times L_{B,\rm tot}$.

Moreover, when comparing results in the B band with those in the B_j band, we assume that $(L_{Bj}/L_{Bj,\odot})/(L_B/L_{B,\odot}) = 1.1$ in agreement with the relation $B_j - B = 0.28(B-V)$ of Blair & Gilmore (1982) (see also Metcalfe, Fong, & Shanks 1995; Maddox, Efstathiou, & Sutherland 1990), where we take $(B_j-B)_\odot = 0.15$ and a mean value of $(B-V) = 0.9$ mag for cluster members.

Finally, we attempt a comparison of the results for those systems cataloged both as NOG groups and as clusters or poor systems (CL+PS). We identify 13 groups for PG and 12 for HG: A194/PG72/HG78, A262/PG102/HG113, A3574/PG753/HG725, Eridanus/PG202/HG207, S373/PG201/HG208, S753/PG770/HG752, S805/PG929/HG898, N67-312/PG581/HG554, N79-298/PG605/HG581, N67-336/PG776/HG753, N67-325/PG787/HG766, N67-326/PG809, N34-171/PG896, HCG62/HG646. Both mass and luminosity of NOG groups correlate with the corresponding CL+PS values, but there is a large scatter. As for PGs, masses are comparable and

mass-to-light ratios are slightly larger: M_{PG}/M_{CL+PS} =0.91 (0.70–1.95) and $(M/L)_{PG}/(M/L)_{CL+PS}$ =1.36 (0.78–1.71), median values with 90% c.l. error bands. As for HGs, masses are smaller and mass-to-light ratios comparable: $M_{HG}/M_{CL+PS} = 0.48$ (0.35–0.63) and $(M/L)_{HG}/(M/L)_{CL+PS} = 0.87$ (0.44–1.58). However, the sample is so small and sparse that this comparison is not useful for understanding which catalog is the more consistent with the treatment of other galaxy systems.

3.5. *The Combined Sample*

Our comparison between groups and other systems does not enable us to express a preference to one or the other of the two NOG catalogs (cf. the above section). Indeed, both algorithms present known problems. It has been suggested that the drawback of percolation methods is the inclusion in the catalogs of possible nonphysical systems, like a long galaxy filament aligned close to the LOS, which could give large mass estimates, while the drawback of hierarchical methods is the splitting of galaxy clusters into various subunits, which give small mass estimates (e.g., Gourgoulhon, Chamaraux, & Fouquè 1992; Giuricin et al. 2000). Therefore, we choose to consider only common groups, i.e., those groups which are identified by both the algorithms (cf. cross-identifications of Tables 5 and 7 of Giuricin et al. 2000), averaging the corresponding estimates of physical quantities. Avoiding PGs which are split into two or more HGs and, vice versa, groups with null mass, as well as groups which are already present in the CL+PS sample, we obtain 296 groups.

Moreover, the physical reality of the very poor detected groups has often been discussed in the literature. In particular, the efficiency of the percolation algorithm has been repeatedly checked in the literature, showing that an appreciable fraction of the poorer groups, those with $N_m < 5$ members, is false (i.e., unbound density fluctuations), whereas the richer groups almost always correspond to real systems (e.g., Ramella, Geller, & Huchra 1989; Ramella et al. 1995; Mahdavi et al. 1997; Nolthenius, Klypin, & Primack 1997; Diaferio et al. 1999). Therefore, among the 296 common groups we consider the 132 groups having more than five members (hereafter GROUP sample). By combining GROUPs with other systems we obtain a fiducial combined sample of 294 systems (CL+PS+GROUP).

4. RESULTS

We computed the values of the mass-to-light ratio for all systems. As for clusters and poor systems, we average COSMOS and APS luminosities when both are available, and then we average the two alternative luminosity estimates, $L_{B,c}$ and $L_{B,f}$, to obtain a single value for each system. In particular, for clusters we consider values coming from G00, too. In Table 5 we list the values of M and M/L for all 294 systems of the combined sample.

Table 6 summarizes our results, listing the median values of M and M/L, and 90% c.l., for all the samples we consider. The general feeling is that M/L_B increases with system mass (cf. Fig. 8).

For a more quantitative analysis we avoid of fitting the behavior of M/L versus M or L because M/L is defined as a function of M and L, and therefore that would mean working with correlated quantities (cf. Mezzetti, Giuricin, & Mardirossian 1982; Girardi et al. 1996). Rather, we directly examine the M-L relation.

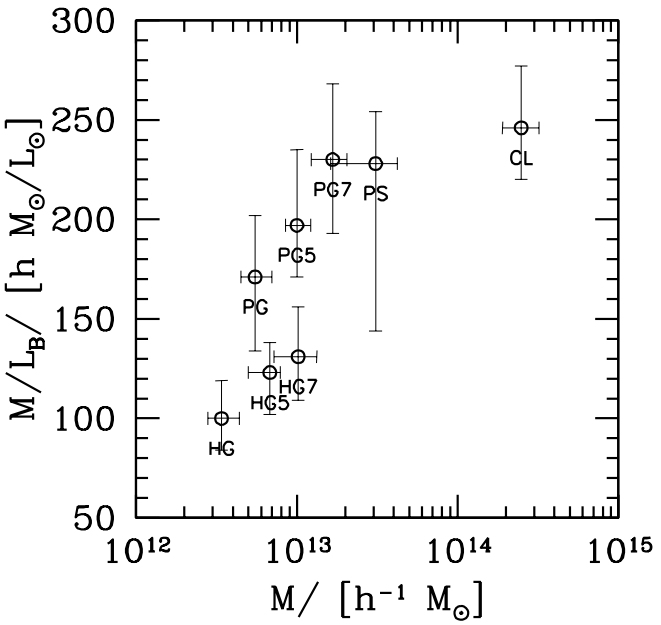

FIG. 8.—Behavior of mass-to-light ratio vs. cluster mass for the sample of clusters (CL), poor systems (PS), and percolation and hierarchical NOG groups of different richness (PG and HG, respectively). Circles are median values with 90% c.l. error bars.

First, we consider together clusters and poor systems, analyzing a combined sample (CL+PS) of 162 systems. Figure 9 shows the M versus L_{B_j} relation. As the errors are comparable, we fit the regression line into the logarithmic plane by using the unweighted bisecting fit (cf. Isobe et al.

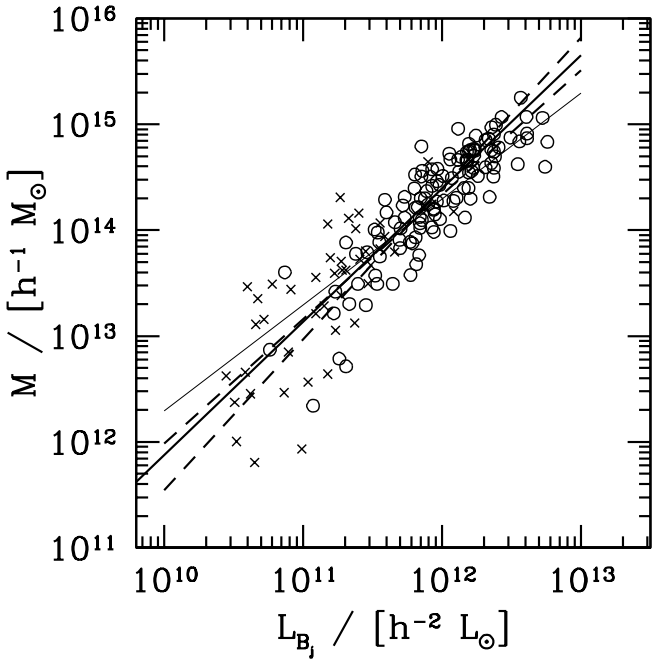

FIG. 9.—Relation between mass and luminosity for the combined sample of clusters (CL, *circles*) and poor systems (PS, *crosses*). Heavy lines represent the linear fits: dashed lines give the direct and the inverse fits, while the solid line gives the bisecting line. The faint line is the $M \propto L_{B_j}$ relation.

TABLE 5

M/L VALUES FOR THE COMBINED SAMPLE

Name (1)	$lg\left(\frac{M}{M_\odot}\right), \frac{M/L_B}{(M/L_B)_\odot}$ (2)	Name (3)	$lg\left(\frac{M}{M_\odot}\right), \frac{M/L_B}{(M/L_B)_\odot}$ (4)	Name (5)	$lg\left(\frac{M}{M_\odot}\right), \frac{M/L_B}{(M/L_B)_\odot}$ (6)
A85	14.99, 445	A119	14.40, 191	A193	14.58, 490
A194	13.78, 274	A229	14.30, 315	A256	14.19, 198
A262	14.12, 99	A295	13.89, 145	A400	14.40, 433
A420	13.88, 413	A458	14.74, 401	A496	14.50, 427
A514	14.91, 376	A524	13.30, 103	A978	14.37, 332
A999	13.49, 100	A1060	14.28, 204	A1069	13.88, 136
A1142	14.29, 552	A1146	14.87, 199	A1185	14.02, 167
A1228	12.79, 37	A1314	13.49, 78	A1631	14.70, 328
A1644	14.65, 325	A1656	14.70, 227	A1795	14.77, 384
A1809	14.66, 338	A1983	14.22, 271	A1991	14.27, 222
A2029	14.83, 131	A2040	14.24, 243	A2048	14.40, 178
A2079	14.67, 391	A2092	14.12, 212	A2107	14.42, 340
A2124	14.84, 210	A2142	15.25, 533	A2151	14.75, 361
A2197	14.55, 296	A2199	14.76, 277	A2353	14.31, 103
A2362	13.79, 236	A2401	13.98, 121	A2426	13.68, 80
A2500	14.01, 340	A2554	14.78, 261	A2569	14.30, 292
A2589	13.89, 239	A2634	14.63, 210	A2644	12.87, 142
A2670	14.74, 391	A2715	14.23, 361	A2717	14.17, 408
A2721	14.74, 257	A2734	14.53, 579	A2755	14.82, 461
A2798	14.28, 172	A2799	14.07, 285	A2800	13.98, 304
A2877	14.69, 394	A2911	14.20, 200	A3093	13.91, 180
A3094	14.67, 450	A3111	12.71, 28	A3122	14.79, 960
A3126	14.89, 491	A3128	14.85, 380	A3142	14.72, 518
A3151	13.29, 76	A3158	14.97, 454	A3194	14.87, 373
A3223	14.51, 355	A3266	15.07, 480	A3334	14.58, 450
A3354	13.76, 94	A3360	14.96, 768	A3376	14.56, 557
A3381	13.57, 124	A3391	14.56, 244	A3395	14.76, 393
A3528N	13.99, 94	A3532	14.51, 198	A3556	14.54, 246
A3558	15.06, 240	A3559	14.10, 145	A3571	14.91, 220
A3574	14.15, 175	A3651	14.59, 210	A3667	15.07, 320
A3693	13.93, 146	A3695	14.59, 180	A3705	14.88, 267
A3733	14.46, 346	A3744	14.10, 192	A3809	14.21, 279
A3822	14.62, 132	A3825	14.59, 255	A3879	13.83, 149
A3880	14.76, 371	A3921	14.31, 175	A4008	14.02, 227
A4010	14.43, 305	A4053	14.31, 421	A4067	14.03, 139
AWM4	12.34, 20	S1157/C67	14.51, 498	CL2335-26	14.60, 79
DC0003-50	13.75, 174	Eridanus	13.60, 597	MKW1	13.22, 109
MKW6A	13.42, 169	S84	13.58, 70	S373	13.49, 138
S463	14.30, 137	S721	14.49, 290	S753	14.12, 268
S805	14.06, 184	S987	14.51, 151	S49-145	13.82, 204
S49-142	12.37, 81	N45-384	13.21, 144	N34-172	13.55, 317
N56-393	13.59, 254	N79-278	13.28, 149	N67-312	12.46, 44
N56-371	13.62, 242	N79-280	11.93, 10	N56-392	12.57, 37
N79-298	12.66, 130	N79-299B	13.67, 167	N67-335	14.06, 836
N79-299A	13.80, 247	N79-283	13.79, 150	N79-292	13.47, 814
N67-333	13.73, 229	N67-323	11.81, 16	N67-317	13.16, 302
N79-270	12.45, 75	N79-296	14.01, 472	N67-329	12.85, 100
N79-297	13.05, 73	N79-276	14.31, 1215	N67-336	13.49, 116
N67-325	13.38, 141	N67-326	13.44, 369	N67-309	13.71, 299
N56-394	13.74, 384	N56-395	14.16, 633	N56-381	13.35, 524
N45-381	12.64, 32	N45-363	14.07, 359	N45-389	14.65, 615
N34-171	13.11, 311	N34-175	14.18, 136	NGC 533	14.11, 670
HCG 42	13.12, 62	NGC 4325	13.49, 565	HCG 62	13.94, 248
NGC 5129	13.62, 228	NGC 491	12.00, 34	NGC 664	12.62, 166
HG3	12.74, 53	HG11	13.52, 645	HG31	12.59, 35
HG49	12.74, 53	HG57	12.53, 32	HG63	13.07, 149
HG83	12.37, 52	HG73	13.72, 263	HG94	12.45, 51
HG109	12.67, 59	HG120	12.95, 127	HG123	12.94, 72
HG138	11.34, 4	HG158	11.83, 21	HG165	11.80, 51
HG167	12.57, 59	HG175	12.59, 72	HG178	12.70, 97
HG185	13.23, 631	HG187	12.87, 125	HG200	12.36, 133
HG201	12.46, 98	HG212	13.41, 211	HG214	12.94, 275
HG223	11.69, 29	HG226	13.11, 190	HG232	12.98, 124

TABLE 5—*Continued*

Name (1)	$lg\left(\frac{M}{M_\odot}\right), \frac{M/L_B}{(M/L_B)_\odot}$ (2)	Name (3)	$lg\left(\frac{M}{M_\odot}\right), \frac{M/L_B}{(M/L_B)_\odot}$ (4)	Name (5)	$lg\left(\frac{M}{M_\odot}\right), \frac{M/L_B}{(M/L_B)_\odot}$ (6)
HG234	12.77, 30	HG246	12.85, 89	HG249	12.80, 291
HG246	12.94, 84	HG261	13.28, 188	HG309	13.11, 135
HG311	12.68, 109	HG322	11.93, 53	HG331	12.65, 84
HG333	11.82, 67	HG348	13.81, 608	HG348	13.64, 539
HG349	12.46, 16	HG361	12.38, 75	HG374	12.66, 102
HG402	12.36, 65	HG421	12.34, 30	HG429	11.99, 66
HG439	12.44, 283	HG454	12.13, 83	HG465	11.71, 38
HG473	14.18, 450	HG507	12.84, 137	HG490	12.12, 49
HG491	12.10, 167	HG500	12.54, 132	HG508	13.11, 165
HG511	12.85, 660	HG507	12.79, 111	HG525	12.45, 100
HG546	13.03, 828	HG545	13.48, 184	HG550	12.64, 88
HG557	13.29, 168	HG545	13.27, 140	HG566	12.87, 140
HG574	13.39, 176	HG595	12.49, 122	HG580	12.69, 80
HG576	11.73, 9	HG594	12.92, 167	HG595	12.67, 117
HG601	12.27, 24	HG602	13.13, 390	HG610	13.00, 225
HG574	13.15, 189	HG607	13.47, 582	HG608	14.09, 425
HG611	13.09, 147	HG610	13.21, 296	HG614	11.71, 97
HG617	12.20, 161	HG619	13.75, 753	HG622	14.53, 859
HG623	12.27, 57	HG626	12.37, 36	HG630	12.32, 35
HG636	13.22, 329	HG647	12.92, 316	HG638	12.41, 25
HG639	11.10, 29	HG641	12.54, 108	HG653	13.02, 189
HG680	12.15, 28	HG690	12.59, 156	HG694	12.94, 184
HG703	12.05, 25	HG704	13.02, 514	HG710	12.93, 72
HG712	11.85, 26	HG718	12.81, 610	HG722	13.29, 118
HG731	13.02, 75	HG737	12.81, 117	HG745	13.26, 278
HG743	12.44, 66	HG745	13.41, 301	HG758	11.89, 71
HG759	12.37, 119	HG806	12.89, 133	HG799	12.66, 51
HG806	13.02, 124	HG806	12.82, 110	HG830	13.30, 395
HG868	12.25, 12	HG872	12.49, 55	HG904	12.68, 151
HG910	13.74, 293	HG910	13.95, 306	HG913	13.78, 185
HG926	13.78, 315	HG939	13.15, 105	HG949	13.85, 590
HG949	13.51, 282	HG959	13.02, 148	HG971	13.38, 171
HG1008	12.60, 63	HG1017	12.75, 276	HG1037	12.68, 60
HG1060	12.31, 35	HG1057	13.55, 481	HG1060	12.29, 24
HG1062	13.35, 197	HG1071	13.02, 180	HG1073	13.40, 309

NOTE.—Table 5 is also available in machine-readable form in the electronic edition of the *Astrophysical Journal*.

1990):

$$\frac{M}{M_\odot} = 10^c \left(\frac{L_{B_j}}{L_{B_j,\odot}}\right)^d . \quad (6)$$

TABLE 6
M/L FOR DIFFERENT SAMPLES

Sample (1)	N_S (2)	M ($10^{13}\,h^{-1}\,M_\odot$) (3)	$M/L_{B_c}, M/L_{B_f}$ [$h\ (M/L_B)_\odot$] (4)	M/L_B [$h\ (M/L_B)_\odot$] (5)
A-CL	52	$20.32^{+5.89}_{-4.71}$	$262^{+43}_{-54}, 238^{+28}_{-51}$	
C-CL[a]	89	$23.39^{+8.85}_{-4.51}$	$276^{+31}_{-32}, 252^{+24}_{-32}$	
CL	119	$24.90^{+7.23}_{-5.87}$	$270^{+32}_{-29}, 245^{+10}_{-32}$	246^{+31}_{-26}
PS	43	$3.09^{+1.12}_{-1.47}$	$223^{+62}_{-80}, 222^{+29}_{-86}$	228^{+26}_{-84}
PG	513	$0.55^{+0.15}_{-0.10}$		171^{+31}_{-37}
PG5	208	$1.00^{+0.22}_{-0.15}$		197^{+38}_{-26}
PG7	112	$1.67^{+0.38}_{-0.44}$		230^{+38}_{-37}
HG	475	$0.34^{+0.10}_{-0.06}$		100^{+19}_{-16}
HG5.....	190	$0.68^{+0.11}_{-0.18}$		123^{+15}_{-21}
HG7.....	103	$1.02^{+0.31}_{-0.30}$		131^{+25}_{-22}
GROUP.....	132	$0.63^{+0.15}_{-0.15}$		122^{+15}_{-20}

[a] We report here the values obtained by G00 for clusters by using COSMOS.

We obtain $c = -1.476 \pm 0.756$ and $d = 1.321 \pm 0.063$. Similar results are obtained by considering $L_{B_j,c}$ and $L_{B_j,f}$ separately, i.e., $d = 1.312 \pm 0.07$ and $d = 1.293 \pm 0.056$, respectively, both larger than one at more than the $3\,\sigma$ level.

Then we extend our analysis to NOG groups. Figure 10 combines results for all NOG groups with those for the CL+PS systems. Both NOG catalogs turn out to show a continuity with other systems, although PGs seem to have larger M/L ratios.

The analysis of our fiducial, combined sample of 294 systems (CL+PS+GROUP), which considers only groups common to both PG and HG catalogs with at least five members, gives

$$\frac{M}{M_\odot} = 10^{-1.596\pm0.381} \cdot \left(\frac{L_B}{L_{B,\odot}}\right)^{1.338\pm0.033} . \quad (7)$$

Similar results are obtained if we consider also all common groups ($d = 1.349 \pm 0.028$ for a combined sample of 458 systems), or those with at least seven members ($d = 1.309 \pm 0.036$ for a combined sample of 231 systems).

Although the above straight line approach can be very useful to show that mass increases faster than luminosity, it might not be adequate to describe the M-L relation in such a wide dynamical range, from poor groups to very rich clus-

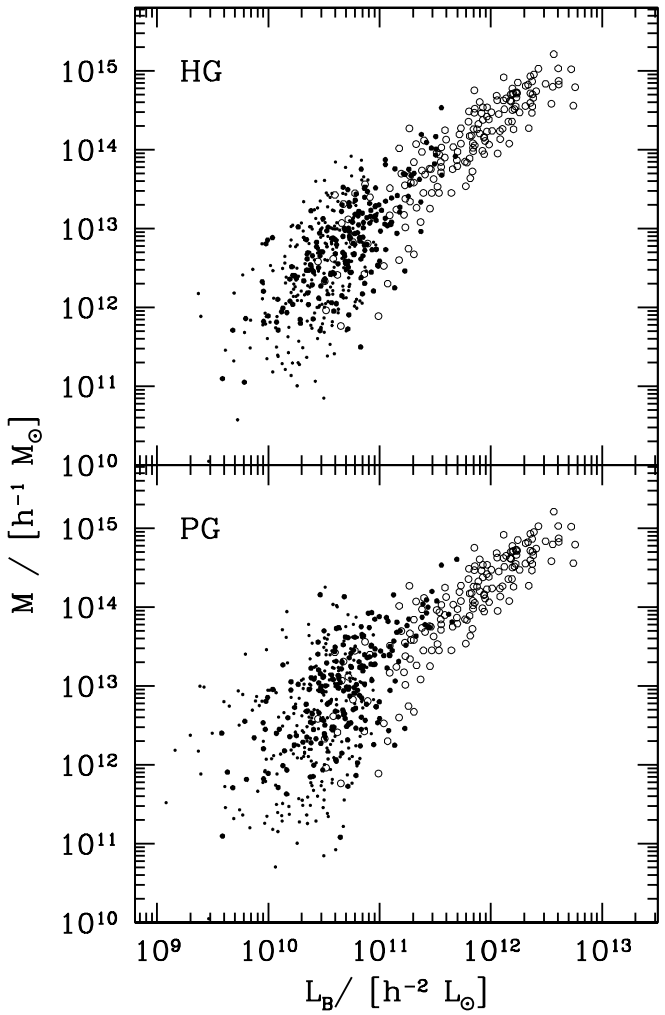

FIG. 10.—Relation between mass and luminosity for groups (*solid circles*, the largest ones for groups with at least five members) and other systems (*open circles*). Both HG and PG catalogs are represented (*top and bottom panels, respectively*).

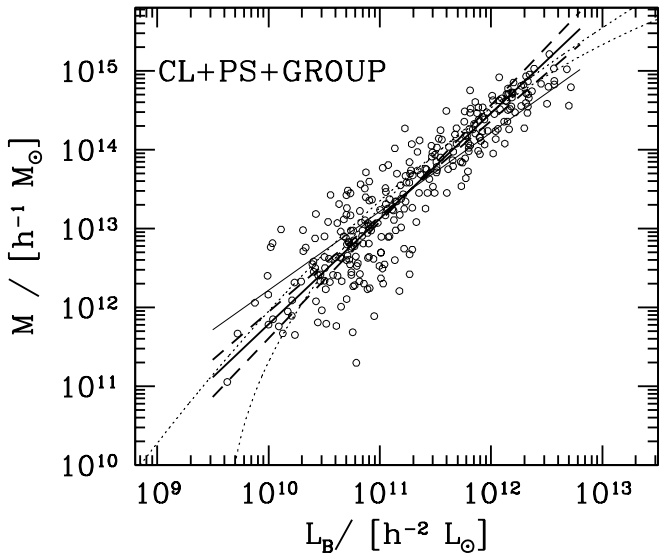

FIG. 11.—Relation between mass and luminosity for our combined sample of clusters, poor systems, and NOG groups. Heavy lines represent the linear fits: dashed lines give the direct and the inverse fits, while the solid line gives the bisecting line. The faint solid line is the $M \propto L_B$ relation. The two faint dotted lines represent the two quadratic fits obtained by minimizing the scatter on one or the other variable.

ters. We also attempt a quadratic fit for the two extreme situations; minimizing the scatter on M-axis we obtain

$$lg(M/M_{\odot}) = -17.04 + 4.26 \cdot lg(L_B/L_{B,\odot}) - 0.14 \cdot lg(L_B/L_{B,\odot})^2 , \quad (8)$$

and minimizing the scatter on L-axis we obtain

$$lg(L_B/L_{B,\odot}) = 17.16 - 1.61 \cdot lg(M/M_{\odot}) + 0.09 \cdot lg(M/M_{\odot})^2 . \quad (9)$$

The first quadratic fit very closely resembles the direct linear fit, while the second one shows a more pronounced change in the slope of the M-L relation; both fits show a steeper slope in the low-mass range (cf. Fig. 11). The above results are obtained by imposing on the dependent variable the same percent errors as masses. Other fits with fixed errors (e.g., of 50% or 80%) give different numerical results but with the same qualitative behavior. Only by having a better knowledge of error on group quantities could we arrive at more conclusive results. In particular, although we have not found any statistical confirmation of this, we suspect that in the case of groups the errors on mass could be larger than the nominal statistical ones, being due to spurious groups and/or interlopers, and thus larger (in percent terms) than the errors on luminosity. This possibility could explain the visual impression for a left vertical selection boundary in the plots of M versus L.

5. DISCUSSION

5.1. *Comparison with Previous Results*

Our estimate of M/L (A-CL) for clusters is fully consistent with that obtained by G00 (C-CL); we refer to G00 for other useful discussions about clusters. As for poor systems, recent studies give values of $M/L_B = 188$–$254\ h\ M_{\odot}\ L_{\odot}^{-1}$ for groups with $\sigma_v = 164$–274 km s^{-1} (Ramella, Pisani, & Geller 1997; Tucker et al. 2000; Carlberg et al. 2001a; Hoekstra et al. 2001a). These results are roughly consistent with richer NOG groups, PG5 and PG7, which have comparable σ_v (cf. Table 4), while the whole NOG group catalogs, which describe the local universe very deeply, are, as expected, characterized by less massive systems, with smaller M/L.

As for the M-L relation, analyzing 89 clusters with homogeneous mass and luminosity estimates, G00 found that mass has a slight but significant tendency to increase faster than the luminosity, $M \propto L_{B_j}^{1.2-1.3}$, where mass and luminosity are computed within the virial radius. Although this result agrees with those indirectly recovered by fundamental plane analyses (Schaeffer et al. 1993; Adami et al. 1998a), there is a general absence of direct evidence for a correlation between M/L and cluster properties (e.g., Dressler 1978; David et al. 1995; Carlberg et al. 1996; Fritsh & Buchert 1999; but see Adami et al. 1998b). G00 pointed out the need for a rather large sample spanning a large dynamical range and homogeneous analysis to detect such a small effect.

Here, with respect to G00, we consider a sample 3 times larger and covering a wider dynamical range (~2 times

larger in logarithmic scale). Our results are fully consistent with those obtained by G00, but with a stronger statistical significance ($\sim$10 σ vs. $\sim$3 σ, according to face values). Interestingly, these results have found support in some independent recent studies. As for groups identified in CNOC2, Carlberg et al. (2001a) find evidence that M/L increases with increasing group velocity dispersion, and Hoekstra et al. (2001a) have noted that the typical group M/L is smaller than that of CNOC clusters (Carlberg et al. 1996). However, the issue is far from being clear: e.g., Hradecky et al. (2000) have recently claimed that M/L is roughly independent of system mass (but, indeed, the seven points in their Fig. 5 could also allow an increase of M/L).

New insights could come from a very different approach, i.e., from preliminary results of the correlation between the red galaxy distribution and the dark matter distribution as measured by the lensing signal (Hoekstra et al. 2001b; Wilson, Kaiser, & Luppino 2001). Pioneering results support the hypothesis that red light traces mass on scales from 0.2 h^{-1} Mpc to very large scales and it is probable that in the future it will be possible to make a comparison with dynamical results.

5.2. *Reliability and Caveats of Observational M/L*

As for the robustness of our results, several tests for luminosity estimates were computed by G00 in their cluster analysis (cf. their § 6.3). In particular, they showed the small effect of changing the analytical form and/or the parameters of the luminosity function in the extrapolation to faint galaxies. Here, this correction is very small for groups and poor systems, which are very close and so very deeply sampled.

Indeed, as for luminosity estimates, the most important correction concerns the fore/background problem, and, in fact, following G00, we use two alternative corrections, leading to two alternative luminosity estimates ($L_{B_j,c}$, and $L_{B_j,f}$ in § 3.2).

In dealing with poor, possibly spiral rich, galaxy systems, it is worthwhile discussing the correction applied for the internal reddening of galaxies, although this is often neglected in analyses of the M/L ratio for galaxy systems (e.g., Hradecky et al. 2000). In this study, following G00, we adopt a mean correction of $A_{B_j} = 0.1$ mag for clusters: this is a compromise between the mean correction of $A_B \sim 0.3$ mag for galaxies of the Third Reference Catalog and the value of $A_B = 0$ mag for early-type galaxies (de Vaucouleurs et al. 1991). As for loose groups of NOG, where the fraction of early galaxies is comparable to that of the field ($f_e \sim 0.2$), the adopted magnitudes are already corrected for internal absorption (Paturel et al. 1997; cf. also Bottinelli et al. 1995). The recent study by Tully et al. (1998) on global extinction agrees with corrections suggested by de Vaucouleurs et al. (1991) and Bottinelli et al. (1995): they find negligible extinction in lenticulars and $A_B \sim 1.8$ in highly inclined spirals (cf. $A_B \sim 1.5$–1.67 by de Vaucouleurs et al. 1991 and Bottinelli et al. 1995). Indeed, some specific studies of highly inclined spiral galaxies could suggest higher extinction values, finding $A_B = 2$–3 mag in the center and then a rapid drop with radius (cf. Jansen et al. 1994, see also Kuchinski et al. 1998). Even supposing that we are underestimating the internal extinction of spirals by a factor of 2, the group M/L is presently overestimated at most by a factor of $\sim$30% and the slope of the M-L relation is presently slightly underestimated (e.g., we would obtain $M \propto L_B^{1.4}$ by applying a 30% correction to NOG group luminosities).

Finally, as for the robustness of our luminosity estimates, we go well beyond G00 results on one particular point. In fact, while G00 results are strongly based on the COSMOS catalog, we have shown that luminosities coming from two different catalogs (COSMOS and APS) are really comparable, suggesting that no systematic effect, connected to a particular catalog, pollutes our results.

The most important systematic uncertainty concerns mass estimates, since our application of the virial theorem assumes that, within each system, mass distribution follows galaxy distribution. For clusters this assumption is supported by several independent analyses using optical and X-ray data, as well as gravitational lensing phenomena (e.g., Durret et al. 1994; Narayan & Bartelmann 1999; Carlberg et al. 1997; Cirimele, Nesci, & Trevese 1997), but we must recognize that the issue is far from being clear for poor systems. The absence of luminosity segregation of galaxies in the velocity space (Giuricin et al. 1982; Pisani et al. 1992) suggests that the effect of dynamical friction in slowing down galaxies with respect to dark matter is very poor. However, analyzing CNOC2 groups, Carlberg et al. (2001a) have recently shown that light might be much more concentrated than mass. If that also galaxy number distribution is more concentrated than mass, our virial mass estimates for very poor systems would be underestimated (Merritt 1987) leading to a steeper M-L relation with respect to the true one. Therefore, we stress that our results are strictly correct only if galaxy distribution traces mass within each individual galaxy system.

In the specific case of groups, one could suspect that the particular selection procedure used biases M/L; i.e., groups having at least three luminous galaxies (with $B < 14$ mag) could be on average more luminous and so with systematically smaller M/L. In order to check for this possible bias, we consider several subsamples of groups having a progressively higher luminosity for the third-brightest galaxy: i.e., groups with at least three galaxies more luminous than 13.5 mag (13.0 mag, 12.5 mag, 12.0 mag). For percolation groups, having median $M/L_B = 171\ h\ M_\odot\ L_\odot^{-1}$, we obtain for the subsamples, respectively: $M/L_B = 173$, 174, 158 $h\ M_\odot\ L_\odot^{-1}$; and for hierarchical groups, having median $M/L_B = 100\ h\ M_\odot\ L_\odot^{-1}$, we obtain $M/L_B = 109$, 104, 119 $h\ M_\odot\ L_\odot^{-1}$. Since there is not a clear trend for a systematic decrease of M/L, we expect that this bias, if any, is negligible.

Unfortunately, our results are not connected in any obvious way to the relation between stellar and total mass in galaxy systems. Indeed, it would be more appropriate to make a direct analysis based on infrared light, which seems a better tracer of stellar mass (e.g., Gavazzi, Pierini, & Boselli 1996). Here we only attempt to infer some conclusions, after discussing the morphological content of different systems.

As for clusters, it is well known that the fraction of late-type galaxies decreases with the local density (Dressler 1980) and increases with the distance from the cluster center (Whitmore, Gilmore, & Jones 1993). In fact, clusters are characterized by the presence of color gradients in the radial direction (Abraham et al. 1996; cf. also Fairley et al. 2001). When working within a physical radius, rather than in a fixed spatial radius, the morphology content seems to be roughly independent of mass (e.g., Whitmore et al. 1993;

Fairley et al. 2001). In this context, our analysis performed within the virial radius suggests that we are dealing with comparable galaxy populations, so that our observed *M-L* relation should also be valid in other magnitude bands.

The situation could be different for poor systems, where the question is far from being clarified. For instance, it is not clear if systems with very low X-ray luminosity are characterized by a very small fraction of bulge-dominated and/or red galaxies; cf. Balogh et al. 2001 and Fairley et al. 2001 for different results. As for loose groups, Carlberg et al. (2001b) have shown the presence of color gradients in massive galaxy groups and Tran et al. (2001) have found evidence for a morphology-radius relation in X-ray detected groups, similar to that of clusters. Instead, no trace of color gradients has been found for less massive groups (Carlberg et al. 2001b). In our case, the fraction of early galaxies in NOG groups is comparable with that of the field ($f_e \sim 0.2$, to be compared to $f_e \sim 0.5$–0.75 in clusters, e.g., Oemler 1974). This could mean that NOG groups are different from clusters in their morphological content or that they are similar, but we are looking at the combined effect of color gradients and a sampling area that is very large with respect to clusters ($\sim 2 \times R_{\rm vir}$). Whatever the reality is, one needs to apply a correction to pass from blue to infrared luminosities.

Assuming $(B-H) \sim 3.75$ and ~ 3.0 for early-type and late-type galaxies, respectively (Fioc & Rocca-Volmerange 1999), as well as $(B-H)_{\odot} = 2.1$ (Wamsteker 1981), we find that $L_H^e = 4.6 L_B^e$ for luminosity of early-type galaxies and $L_H^l = 2.3 L_B^l$ for luminosity of late-type galaxies. Then, when assuming that typical blue galaxy luminosities in clusters are roughly comparable for early- and late-type galaxies (e.g., Sandage, Binggeli, & Tammann 1985; Andreon 1998) and that the early galaxy fraction goes from 0.75 to 0.2 for spiral-poor clusters and groups, respectively, we obtain $L_H \sim 4.0 L_B$ and $L_H \sim 2.8 L_B$ for clusters and groups, respectively. Therefore, we expect that M/L_H for groups (GROUP sample) will still be lower than for clusters (CL sample, cf. Table 6) by $\sim$40%, compared with a factor of 2 difference in M/L_B.

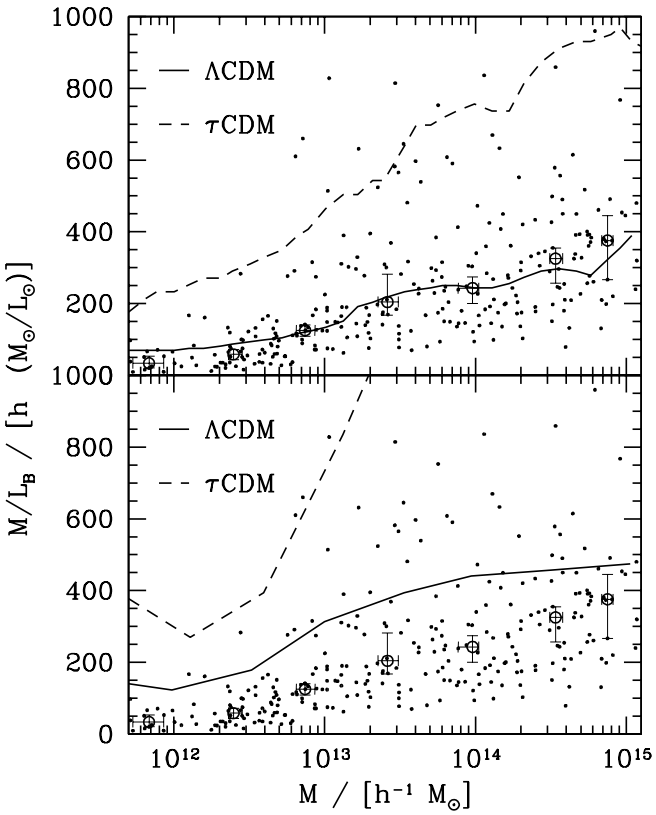

FIG. 12.—Comparison between the observational behavior of mass-to-light of galaxy systems and the theoretical predictions of Kauffmann et al. (1999, *top panel*) and Benson et al. (2000, *bottom panel*); see text. When plotting the Kauffmann et al. results we assume a closure value for the universe $M/L_B[\text{universe}] = 1350\ h\ M_{\odot}\ L_{\odot}^{-1}$ (from the luminosity density $\rho_l \sim 2 \times 10^8\ h\ L_{\odot}\ \text{Mpc}^{-3}$ by Efstathiou et al. 1988). For comparison, Benson et al. quoted a mean value of $M/L_B = 1440\ h\ M_{\odot}\ L_{\odot}^{-1}$ in their simulation as a whole in the τCDM cosmology. Points represent individual data for our combined sample, while circles show median values with 90% c.l. error bands.

5.3. *Comparison with Theoretical Results*

The assumption that M/L within galaxy clusters is typical of the universe as a whole leads to an estimate of the matter density parameter Ω_m, i.e., $\Omega_m = (M/L) \cdot \rho_L/\rho_c$, where ρ_c is the critical density, and ρ_L is the typical luminosity density of the universe, as generally determined on field galaxies (Oort's method, e.g., Bahcall et al. 1995; Carlberg et al. 1996; G00). However, both assumptions that luminosity is conserved when field galaxies fall into a cluster and that galaxy formation is the same in all environments are questionable. Recently, the combination of cosmological numerical simulations and semianalytic modeling of galaxy formation have faced the question of galaxy systems M/L in a more realistic way (e.g., Kauffmann et al. 1999; Bahcall et al. 2000; Benson et al. 2000; Somerville et al. 2001). Here we attempt a comparison with the theoretical results.

Figure 12 compares our observational results with the theoretical predictions of Kauffmann et al. (1999) and Benson et al. (2000), who both recovered the behavior of M/L_B versus halo mass of galaxy systems in the framework of cold dark matter (CDM) models for two alternative cosmologies: a low-density model with $\Omega_m = 0.3$ and $\Omega_\Lambda = 0.7$ (ΛCDM), and a high-density model with $\Omega_m = 1$ and shape parameter $\Gamma = 0.21$ (τCDM).

The $\Omega_m = 1$ cosmology is reported here for the sake of completeness. Also without taking into account the small-mass range, where we should recompute the mass of NOG groups for this kind of model, $\Omega_m = 1$ cosmology is clearly rejected according to the our observational results.

However, the preferred value of Ω_m is not obvious, since the model with $\Omega_m = 0.3$ by Kauffmann et al. fits the data well, while the results of Benson et al. suggest a smaller value. Indeed, the predicted value of M/L shows large differences among the predictions of different authors and can vary considerably in many theoretical details, e.g., the correction of dust extinction (cf. Somerville et al. 2001). Besides normalization, the whole behavior of M/L can also be very useful in constraining theoretical results: e.g., the results obtained by Kauffmann et al. reproduce the steepness of the observational increase of M/L with halo mass, while the results by Benson et al. show a flatter behavior.

Finally, we discuss the very recent results by Marinoni & Hudson (2002), who derive the behavior of M/L by using the analytical approach of Press & Schechter (1974) and the observational luminosity function for galaxy systems: their

prediction for the ΛCDM model agrees well with our findings in the 10^{13}–$10^{14}\,h^{-1}\,M_{\odot}$ range, but they obtain a steeper slope in the high-mass range, and a slope inversion in the low-mass range.

6. SUMMARY AND CONCLUSIONS

We analyze the mass-to-light ratios of galaxy systems from poor groups to rich clusters by considering virial mass estimates and blue band luminosities.

We extend the previous work of G00, where they computed B_j band luminosities derived from the COSMOS catalog (Yentis et al. 1992) for a sample of 89 galaxy clusters, with virial mass homogeneously estimated by G98.

In this study we consider another 52 clusters having virial masses estimated by G98, a sample of 36 poor clusters proposed by L96, and a sample of seven rich groups well analyzed by ZM98. For each poor system we select member galaxies and compute virial mass as performed by G98. For all systems we compute B_j-band luminosity by using both the APS catalog (Pennington et al. 1993) and the COSMOS catalog with the same procedure as that adopted by G00. Both mass and luminosity for each object are computed within the virial radius, in order to consider comparable physical regions for systems of different mass. The advantage of this procedure lies in the fact that one can compare regions with similar dynamical status and galaxy populations. By also taking into account the results of G00, we obtain a sample of 162 galaxy systems having homogeneous mass and luminosity estimates.

To extend our database, we consider the two group catalogs identified in the NOG catalog by Giuricin et al. (2000), based on two different group identification algorithms, a percolation one and a hierarchical one (∼500 groups for each catalog). We compute mass and blue band luminosity for each group, homogenizing our results to those of other systems as much as possible; in particular, we rescale mass and luminosity to the central, possibly virialized, group region.

To avoid possible spurious groups, we consider the subsample of 132 NOG groups identified in both catalogs and having at least five members. We combine these groups with clusters and poor systems to obtain a fiducial combined sample of 294 systems spanning a very large dynamical range ($\sim 10^{12}$–$10^{15}\,h^{-1}\,M_{\odot}$).

We find that mass increases faster than luminosity. By using the bisecting unweighted procedure, the analysis of the combined sample gives

$$\frac{M}{M_{\odot}} = 10^{-1.596\pm0.381}\left(\frac{L_B}{L_{B,\odot}}\right)^{1.338\pm0.033}. \qquad (10)$$

Consistent results are recovered by using the more homogeneous subsample, which contains only 162 clusters and poor systems. This result agrees with that reported by G98, confirming the effect at a higher statistical significance (there the effect was detected at the $\sim 3\,\sigma$ level).

When analyzing the combined sample with a quadratic fitting relation, we find a tendency for a steeper slope in the low-mass range.

Finally, we compare our observational results with the theoretical predictions with the behavior of M/L_B versus halo mass, in particular to the behavior recently predicted by the combination of cosmological numerical simulations and semianalytic modeling of galaxy formation. We find a very good agreement with the result by Kauffmann et al. (1999) for a CDM model with $\Omega_m = 0.3$ and $\Omega_\Lambda = 0.7$. This demonstrates that the study of the mass-to-light ratio scaling for galaxy systems represents a useful tool for constraining models of galaxy formation.

We wish to dedicate this paper to the memory of our friend and colleague Giuliano Giuricin who suddenly died during the preparation of this paper. We thank Andrea Biviano and Stefano Borgani for useful discussions. We thank an anonymous referee for useful suggestions. This research has made use of the APS Catalog of POSSI which is supported by the National Aeronautics and Space Administration and the University of Minnesota[2]; the ROE/NRL UKST Southern Sky Catalog, work funded in part by the Office of Naval Research and by a grant from the NASA ADP program[3]; the COSMOS/UKST Southern Sky Catalog supplied by the Anglo-Australian Observatory; and the NASA/IPAC extragalactic Database (NED), which is operated by the Jet Propulsion Laboratory, California Institute of Technology, under contract to the National Aeronautics and Space Administration. This work has been partially supported by the Italian Ministry of Education, University, and Research (MIUR), and by the Italian Space Agency (ASI).

[2] The database can be accessed at http://aps.umn.edu/.
[3] The database can be accessed at http://xip.nrl.navy.mil/www_rsearch/RS_form.html.

REFERENCES

Abraham, R. G., et al. 1996, ApJ, 471, 694
Adami, C., Mazure, A., Biviano, A., Katgert, P., & Rhee, G. 1998a, A&A, 331, 493
Adami, C., Mazure, A., Katgert, P., & Biviano, A. 1998b, A&A, 336, 63
Andreon, S. 1998, A&A, 336, 98
Allen, S. W. 1997, MNRAS, 296, 392
Bahcall, N. A., Cen, R., Davè, R., Ostriker, J. P., Yu, Q. 2000, ApJ, 541, 1
Bahcall, N. A., Lubin, L. M., & Dorman, V. 1995, ApJ, 447, L81
Balogh, M. L., et al. 2001, preprint (astro-ph/0110326)
Bardeen, J. M., Bond, J. R., Kaiser, N., & Szalay, A. S. 1986, ApJ, 304, 15
Beers, T. C., Flynn, K., & Gebhardt, K. 1990, AJ, 100, 32
Benson, A. J., Cole, S., Frenk, C. S., Baugh, C. M., & Lacey, C. G. 2000, MNRAS, 311, 793
Biviano, A. 2001, in ASP Conf. Ser., Tracing Cosmic Evolution with Galaxy Clusters, ed. S. Borgani, M. Mezzetti, & R. Valdarnini (San Francisco: ASP), in press
Blair, M., & Gilmore, G. 1982, PASP, 94, 742
Blumenthal, G. R., Faber, S. M., Primack, J. R., & Rees, M. J. 1984, Nature, 311, 517
Bottinelli, L., Gouguenheim, L., Paturel, G., & Teerikorpi, P. 1995, A&A, 296, 64
Carlberg, R. G., et al. 1996, ApJ, 462, 32
Carlberg, R. G., Yee, H. K. C., & Ellingson, E. 1997, ApJ, 478, 462
Carlberg, R. G., et al. 2001a, ApJ, 552, 427
Carlberg, R. G., et al. 2001b, ApJ, 563, 736
Colless, M. 1989, MNRAS, 237, 799
Cirimele, G., Nesci, R., & Trevese, D. 1997, ApJ, 475, 11
Danese, L., De Zotti, C., & di Tullio, G. 1980, A&A, 82, 322
David, L. P., Jones, C., & Forman, W. 1995, ApJ, 445, 578
Davis, M., Efstathiou, G., Frenk, C. S., & White, S. D. M. 1985, ApJ, 292, 371
de Vaucouleurs, G., de Vaucouleurs, A., Corwin, H. G., Buta, R. J., Paturel, G., & Fouqué, P. 1991, Third Reference Catalog of Bright Galaxies, (New York: Springer)
Diaferio, A., Kauffmann, G., Colberg, J. M., White, S. D. M. 1999, MNRAS, 307, 537
Diaferio, A., Ramella, M., Geller, M. J., Ferrari, A. 1993, AJ, 105, 2035
Dressler, A. 1978, ApJ, 226, 55

Dressler, A. 1980, ApJ, 236, 351
Durret, F., Gerbal, D., Lachièze-Rey, M., Lima-Nieto, G., & Sadat, R. 1994, A&A, 287, 733
Efstathiou, G., Ellis, R. S., & Peterson, B. A. 1988, MNRAS, 232, 431
Eke, V. R., Cole, S., & Frenk, C., S. 1996, MNRAS, 282, 263
Fadda, D., Girardi, M., Giuricin, G., Mardirossian, F., & Mezzetti, M. 1996, ApJ, 473, 670
Fairley, B. W., Jones, L. R., Wake, D. A., Collins, C. A., Burke, D. J., Nichol, R. C., & Romer, A. K. 2001, preprint (astro-ph/0111169)
Fasano, G., Pisani, A., Vio, R., & Girardi, M. 1993, ApJ, 416, 546
Fioc, M., & Rocca-Volmerange, B. 1999, A&A, 351, 869
Fritsch, C., & Buchert, T. 1999, A&A, 344, 749
Gavazzi, G., Pierini, D., & Boselli, A. 1996, A&A, 312, 397
Girardi, M., Biviano, A., Giuricin, G., Mardirossian, Mezzetti, M., A. 1995, ApJ, 438, 527
Girardi, M., Borgani, S., Giuricin, G., Mardirossian, F., & Mezzetti, M. 1998a, ApJ, 506, 45
———. 2000, ApJ, 530, 62 (G00)
Girardi, M., Fadda, D., Giuricin, G., Mardirossian, F., Mezzetti, M., & Biviano, A. 1996, ApJ, 457, 61
Girardi, M., & Giuricin, G. 2000, ApJ, 540, 45 (GG00)
Girardi, M., Giuricin, G., Mardirossian, F., Mezzetti, M., & Boschin W. 1998b, ApJ, 505, 74 (G98)
Girardi, M., & Mezzetti M. 2001, ApJ, 548, 78
Giuricin, G., Gondolo, P., Mardirossian, F., Mezzetti, M., & Ramella, M. 1988, A&A, 199, 85
Giuricin, G., Mardirossian, F., & Mezzetti, M. 1982, ApJ, 255, 361
Giuricin, G., Mardirossian, F., Mezzetti, M., & Santangelo, P. 1984, ApJ, 277, 38
Giuricin, G., Marinoni, C., Ceriani, L., & Pisani, A. 2000, ApJ, 543, 178
Gourgoulhon, E., Chamaraux, P., & Fouquè, P. 1992, A&A, 255, 69
Guest, P. G. 1961, Numerical Methods of Curve Fitting (Cambridge: Cambridge Univ. Press)
Heydon-Dumbleton, N. H., Collins, C. A., & MacGillivray, H. T. 1988, in Large-Scale Structures of the Universe—Observational and Analytical Methods (Berlin: Springer), 71
———. 1989, MNRAS, 238, 379
Hoekstra, H., Yee, H. K., & Gladders, M. D. 2001a, ApJ, 558, L11
Hoekstra, H., et al. 2001b, ApJ, 548, L5
Hradecky, Jones, C., Donnelly, R. H., Djorgovski, S. G., Gal, R. R., & Odewahn, S. C. 2000, ApJ, 543, 521
Isobe, T., Feigelson, E. D., Akritas, M. G., & Babu, G. J. 1990, ApJ, 364, 104
Jansen, R. A., Knapen, J. H., Beckman, J. E., Peletier, R. F., & Hes, R. 1994, MNRAS, 270, 373
Katgert, P., Mazure, A., den Hartog, R., Adami, C., Biviano, A., & Perea, J. 1998, A&AS, 129, 399
Katgert, P., et al. 1996, A&A, 310, 8
Kauffmann, G., Colberg, Jö, M., Diaferio, A., & White, S. D. M. 1999, MNRAS, 303, 188
Kron, R. G. 1978, Ph.D. thesis, Univ. California, Berkeley
Kuchinski, L. E., Terndrup, D. M., Gordon, K. D., & Witt, A. N. 1998, AJ, 115, 1438
Ledlow, M. J., Loken, C., Burns, J. O., Hill, J. M., & White, R. A. 1996, AJ, 112, 388 (L96)
Lewis, A. D., Ellingson, E., Morris, S. L., & Carlberg, R. G. 1999, ApJ, 517, 587
Limber, D. N., & Mathews, W. G. 1960, ApJ, 132, 286
Lumsden, S. L., Collins, C. A., Nichol, R. C., Eke, V. R., & Guzzo, L. 1997, MNRAS, 290, 119
Maddox, S. J., Efstathiou, G. P., & Sutherland, W. J. 1990, MNRAS, 246, 433
Mahdavi, A., Böringher, H., Geller, M. J., & Ramella, M. 1997, ApJ, 483, 68
Mahdavi, A., Geller, M. J., Böringher, H., Kurtz, M. J., & Ramella, M. 1999, ApJ, 518, 69
Mamon, G. A. 1994, in *N*-body Problems and Gravitational Dynamics, ed. F. Combes & E. Athanassoula (Meudon: Obs. de Paris), 188
Marinoni, C., & Hudson, M. J. 2002, ApJ, in press
Mellier, Y. 1999, in Theoretical and Observational Cosmology: Proc. NATO Advanced Study Institute on Theoretical and Observational Cosmology, Cargese, France, ed. M. Lachièze-Rey (Boston: Kluwer), 211
Merritt, D. 1987, ApJ, 313, 121
———. 1988, in ASP Conf. Ser. 5, The Minnesota Lectures on Clusters of Galaxies and Large-Scale Structures, ed. J. M. Dickey (San Francisco: ASP), 175
Metcalfe, N., Fong, R., & Shanks, T. 1995, MNRAS, 274, 769
Mezzetti, M., Giuricin, G., & Mardirossian, F. 1982, ApJ, 259, 30
Narayan, R., & Bartelmann, M. 1999, in Formation of Structure in the Universe, ed. A. Dekel & J. P. Ostriker (Cambridge: Cambridge Univ. Press), 360
Nolthenius, R., Klypin, A., & Primack, J. R. 1997, ApJ, 480, 43
Odewahn, S. C., & Aldering, G. 1995, AJ, 110, 2009
Odewahn, S. C., Humphreys, R. M., Aldering, G., & Thurmes, P. 1993, PASP, 105, 1354
Oemler, A. Jr. 1974, ApJ, 194, 1
Paturel, G., et al. 1997, A&AS, 124, 109
Pennington, R. L., Humphreys, R. M., Odewahn, S. C., Zumach, W., & Thurmes, P. M. 1993, PASP, 105, 521
Pisani, A. 1993, MNRAS, 265, 706
———. 1996, MNRAS, 278, 697
Pisani, A., Giuricin, G., Mardirossian, F., & Mezzetti, M. 1992, ApJ, 389, 68
Press, W. H., & Schechter, P. 1974, ApJ, 187, 425 (PS)
Ramella, M., Geller, M. J., & Huchra, J. P. 1989, AJ, 344, 57
Ramella, M., Geller, M. J., Huchra, J. P., & Thorstensen, J. R. 1995, AJ, 109, 1469
Ramella, M., Pisani, A., & Geller, M. J. 1997, AJ, 113, 283
Rauzy, S., Adami, C., & Mazure, A. 1998, A&A, 337, 31
Rees, M. J. 1985, MNRAS, 213, P75
Rubin, V. C. 1993, Proc. Nat. Acad. USA, 90, 4814
Sandage, A., Binggeli, B., & Tammann, A. 1985, AJ, 90, 1759
Schaeffer, R., Maurogordato, S., Cappi, A., & Bernardeau, F. 1993, MNRAS, 263, L21
Shanks, T., Stevenson, P. R. F., & Fong, R. 1984, MNRAS, 206, 767
Schechter, P. 1976, ApJ, 203, 297
Schindler, S. 1996, A&A, 305, 756
Somerville, R. S., Lemson, G., Sigad, Y., Dekel, A., Kauffmann, G., & White, S. D. M. 2001, MNRAS, 320, 289
The, L. S., & White, S. D. M. 1986, AJ, 92, 1248
Tran, K.-V. H., Simard, L., Zabludoff, A. I., & Mulchaey, J. S. 2001, ApJ, 549, 172
Tucker, D. T., et al. 2000, ApJS, 130, 237
Tully, R. B., Pierce, M. J., Huang, J.-S., Saunders, W., Verheijen, M. A. W., & Witchalls, P. L. 1998, AJ, 115, 2264
Valotto, C. A., Nicotra, M. A., Muriel, H., & Lambas, D. G. 1997, ApJ, 479, 90
Wamsteker, W. 1981, A&A, 97, 329
White, R. A., Bliton, M., Bhavsar, S. P., Bornmann, P., Burns, J. O., Ledlow, M. J., & Loken, C. 1999, AJ, 118, 2014
Whitmore, B. C., Gilmore, D., M., & Jones, C. 1993, ApJ, 407, 489
Wilson, G., Kaiser, N., & Luppino, G. A. 2001, ApJ, 556, 601
Wu, X. P., & Fang, L. Z. 1997, ApJ, 483, 62
Yentis, D., Cruddace, R., Gursky, H., Stuart, B., Wallin, J., MacGillivray, H., & Collins, C. 1992, in Digitised Optical Sky Survey, ed. H. T. MacGillivray & E. B. Thomson (Dordrecht: Kluwer), 67
Zabludoff, A., & Mulchaey, J. S. 1998a, ApJ, 496, 39 (ZM98)
———. 1998b, ApJ, 498, L5
Zwicky, F. 1933, Helv. Phys. Acta, 6, 10
Zwicky, F., Herzog, E., Karpowicz, M., Kowal, C. T., & Wild, P. 1961–1968, Catalog of Galaxies and Clusters of Galaxies (Pasadena: Caltech)